# Experimental Determination of Track Friction Coefficients

**Roger Cordes, Ph.D., P.E.**
Professor of Practice, Assist. Dept. Head
Department of Ocean Engineering,
Texas A&M University, College Station, College Station, USA.
Email: rcordes@tamu.edu

**Curtis Peña**
M.S. Student
Department of Ocean Engineering,
Texas A&M University, College Station, College Station, USA.
Email: curtis.pena@tamu.edu

**David H. Allen, Ph.D.**
Professor
Department of Ocean Engineering,
Texas A&M University, College Station, College Station, USA.
Email: dhallen@tamu.edu

A Report on Research Sponsored by

University Transportation Center for Railway Safety (UTCRS)

Texas A&M University (TAMU)

September 30, 2025

**Technical Report Documentation Page**

| | | |
|---|---|---|
| 1. Report No.<br>UTCRS-TAMU-I5CY24 | 2. Government Accession No. | 3. Recipient's Catalog No. |
| 4. Title and Subtitle<br><br>Experimental Determination of Track Friction Coefficients | | 5. Report Date<br>September 30, 2025 |
| | | 6. Performing Organization Code<br>UTCRS-TAMU |
| 7. Author(s)<br>R. Cordes, C. Peña, and D. H. Allen | | 8. Performing Organization Report No.<br>CRR-2025-04 |
| 9. Performing Organization Name and Address<br>University Transportation Center for Railway Safety (UTCRS)<br>Center for Railway Research (CRR)<br>Texas A&M University (TAMU)<br>College Station, TX 77843 | | 10. Work Unit No. (TRAIS) |
| | | 11. Contract or Grant No.<br>69A3552348340 |
| 12. Sponsoring Agency Name and Address<br>U.S. Department of Transportation (USDOT)<br>University Transportation Centers Program<br>1200 New Jersey Ave. SE<br>Washington, DC, 20590 | | 13. Type of Report and Period Covered<br>Project Report<br>June 1, 2024 – August 31, 2025 |
| | | 14. Sponsoring Agency Code<br>USDOT UTC Program |
| 15. Supplementary Notes | | |
| 16. Abstract<br>The sliding friction resistance between rail crossties and ballast material was examined. Testing focusing on the equivalent (or average) coefficient of friction spread over the crosstie contact area was performed for high density polyethylene (HDPE) smooth and dimpled crossties as well as for dry and wet wood crossties. Ballast rock included common gravel and two supplied types. The ballast shapes were characterized as were the compressive properties of the ties (in compression perpendicular to the wood, both dry and wet). Indentation tests and finite element models were used to verify the compressive properties and to examine the effect of friction for a direct indention as well as an indention followed by lateral movement, akin to what a crosstie may see when subjected to lateral forces. The results present initial findings relating to material properties and friction properties that could be used to evaluate the effectiveness of crosstie-ballast lateral resistance in different situations, and methods to improve the resistance. | | |
| 17. Key Words<br>Track ballast, Railroad Ties, Friction, Coefficient of Friction | 18. Distribution Statement<br>This report is available for download from https://www.utrgv.edu/railwaysafety/research/infrastructure/index.htm | |
| 19. Security Classification (of this report)<br>None | 20. Security Classification (of this page)<br>None | 21. No. of Pages<br>51 / 22. Price |

## Table of Contents

## List of Figures

## List of Tables

Table Title Page No.

## Disclaimer

The contents of this report reflect the views of the authors, who are responsible for the facts and the accuracy of the information presented herein. This document is disseminated under the sponsorship of the U.S. Department of Transportation's University Transportation Centers Program, in the interest of information exchange. The U.S. Government assumes no liability for the contents or use thereof.


## Acknowledgments

The authors want to acknowledge the University Transportation Center for Railway Safety (UTCRS) for the financial support provided to perform this study through the USDOT UTC Program under Grant No. 69A3552348340.

## Research Overview

The rail track support system for railways includes the foundation, ballast material, the periodic crossties and connection system, and the rail itself. Rail failures from mechanical movements in the rail support system include local rotations and displacements due to locomotive motion, component loosening and cyclic heating and cooling from the environment. Improved rail buckling models (1,2,3) have shed light on the relationships between many of these variables. To provide guidance on the possible ranges and influence of the crosstie-ballast interface, an experimental study was conducted.

The interface between several crossties and several ballast types was examined. Frictional sliding tests were conducted to determine sliding behavior and an equivalent coefficient of friction. These tests were further investigated by examining the local interactions; in a typical interface a small number of ballast rocks provide the majority of the friction as they penetrate the crosstie. A model was used to examine the family of penetrations and their frictional resistance locally and compare the results to the overall frictional behavior. The model showed that the sharpness (facetedness) of the ballast and areal density of penetrations could be related to the macro behavior. This work highlights the differences between high density polyethylene (HDPE), wood, and wet (saturated) wood crossties and 3 types of ballast materials.

## Background

The support structure for railroad rails is a layered system designed to distribute the weight of trains, maintain track alignment, and provide long-term durability under heavy and repeated loads. Above the subgrade or native soil, the typical system consists of the main components: crossties (sleepers), ballast, anchors (fasteners) and spikes (see Figure 1). These function to provide resistance to operational loadings that produce displacements and rotations. The support system effectiveness and fitness-for-service depends on these main components as well as the interaction between these components:

### ***Crossties***

Railroad crossties are structural elements laid perpendicular to the rails and embedded within the ballast layer. Their primary functions are maintaining the correct gauge between rails, distributing loads from trains into the ballast and subgrade, and providing lateral and longitudinal

restraint to the rails. Crossties are manufactured from a variety of materials, including timber, prestressed concrete, and composite polymers, each with unique mechanical and frictional properties that influence track performance and maintenance requirements.

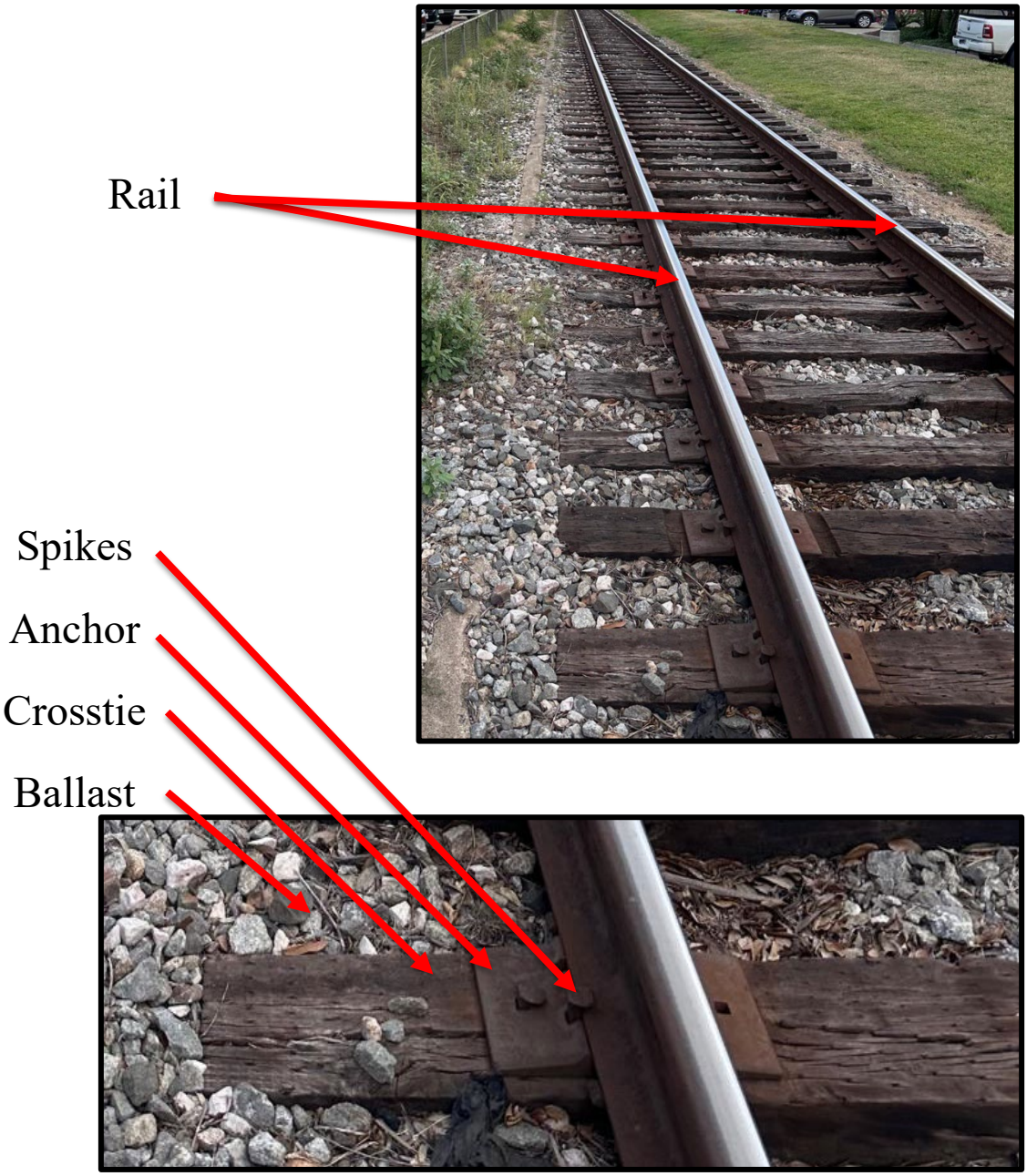


**Figure 1. Rail System and Supporting Components.**

***Ballast***

The ballast provides a stable base for the track and distributes load to the subgrade. Ballast is typically crushed stone (granite or limestone) with a distribution of sizes and pointedness or facetedness. The ballast can be unpacked or tamped and packed around crossties, thereby increasing the frictional resistance to crosstie movement. Ballast wear can be significant over time and influence this behavior and the presence of ground material or fines.

***Anchors and Spikes***

Rail fasteners secure the rails to the crossties to ensure proper alignment and stability. There are a number of types of rail fasteners and connection systems: spikes are commonly used and are hammered directly into wood ties, screw spikes are threaded and provide greater holding resistance than spikes, and clip systems are used, especially with concrete ties. By anchoring the rails in place, crossties resist lateral movements and rotations that can lead to track instability, such as rail buckling under thermal expansion or repeated loading.

When viewed as a support system, all of these components need to be understood in terms of their properties and their interface properties as they touch or are mechanically affixed to another component. The variations in properties and in interfacial properties need to be better understood to minimize the risk of track failures from mechanical loss of support (e.g., from track buckling or ballast movements). Inspection protocols need to address the health of each of the components and fitness-for-service of the system with an understanding of the acceptable ranges of properties and behaviors such as crosstie-ballast friction in dry and wet environments.

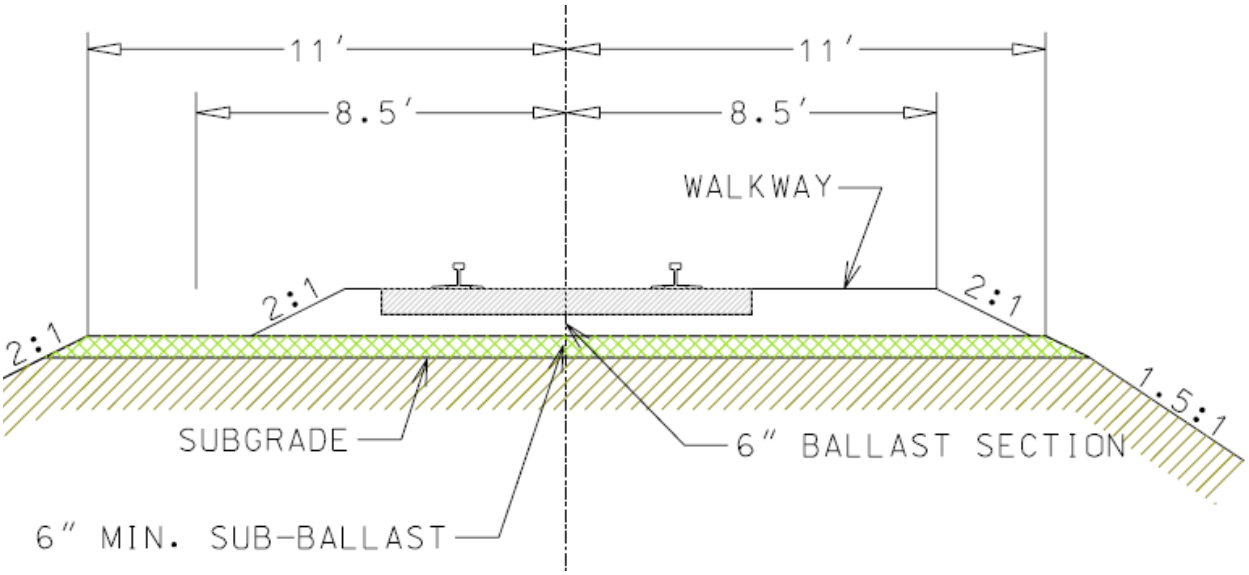


**Figure 2. Ballast-Crosstie Support (4).**

## Experimental and Modeling Approach

The experimental work began focusing on the friction between various types of crossties and various types of ballast. These results are summarized near the end of this report. That work included the contact behavior at the interface of the ballast and a crosstie. To clarify the global frictional response, the behavior at a local level was examined. This was accomplished by first establishing the material properties of the crossties in compression and then examining how a single ballast rock would push into and slide along the different crossties. Experimental and numerical (finite element) methods were used to verify the material and frictional properties and their distribution.

The pushing of a crosstie onto ballast is often simplified as the overall force on a crosstie uniformly distributed to the crosstie-ballast interface. Similarly, the sliding of a crosstie over ballast is often simplified as an average interfacial shear and a related average interfacial coefficient of friction (i.e., Coulomb friction). To clarify the actual interfacial contact behavior, impressions were made and the average number of contact points from ballast was quantified. The belief is that the sliding behavior of a crosstie over ballast is less like a crosstie sliding over a uniform interface and more like a crosstie sliding with a finite number of poking rocks that dig into the crosstie and cause the majority of the lateral sliding resistance.

The overall flow of the model is shown in Figure 3. As will be discussed, for each material or interfacial property, there is a distribution; when dealing with large-grained wood ties the scatter in compressive properties and in friction can be large because of the scale of the event compared to the scale of the wood grain size.

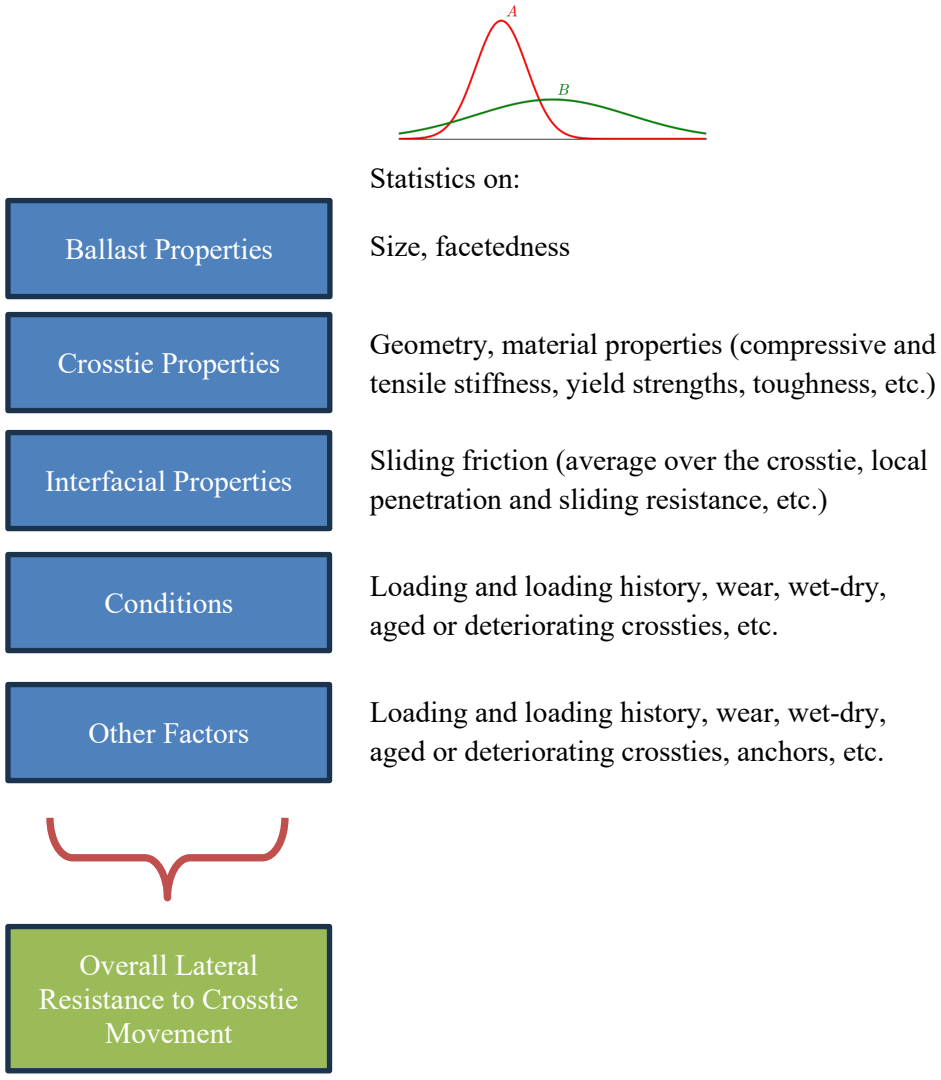


**Figure 3. Influence of Component Properties on the Overall Sliding Resistance of a Crosstie.**

**Results to Date: Ballast Characterization**

Three types of ballast material were examined: common gravel (#0) and two from BNSF. Photos of the ballast material are shown in Figure 4. 125 individual rocks from each were examined individually to produce the data shown in Table 1. In the table, the relatively small size of common gravel can be seen in the volume comparison. Of interest to the ballast-crosstie contact is the relative sharpness of the rocks; the facetedness can be quantified by the flatness index, elongation index, and sphericity with definitions:

$$Flatness\ Index = \left[\frac{S}{L}\right]$$

$$Elongation\ Index = \left[\frac{I}{L}\right]$$

$$Sphericity = \left[\frac{S * I * L}{L^3}\right]^3$$

Dimensions arranged as L > I > S

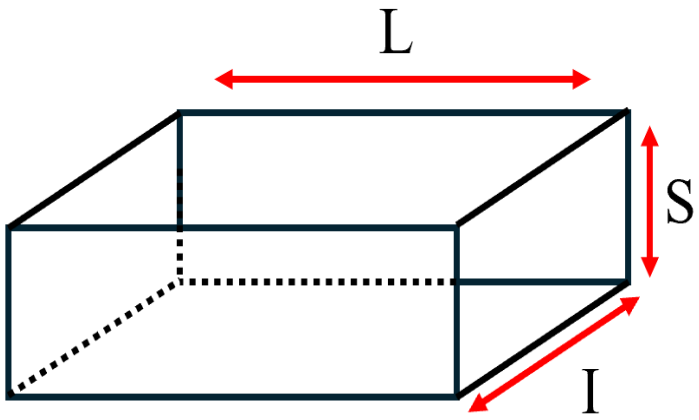


These definitions imply that the values should tend toward:

0 (very sharp rock) < Flatness Index < 1.0 (perfectly round or square rock)

0 (very sharp rock) < Elongation Index < 1.0 (perfectly round or square rock)

0 (very sharp rock) < Sphericity < 1.0 (perfectly round or square rock)

#0 #1 #2

**Figure 4. Photos of Ballast.**

**Table 1: Ballast Characterization Results**

| | Flatness Index [S/L] [closer to 0 means the rock is flatter] | | | | |
|---|---|---|---|---|---|
| **Ballast #** | Min. | Mean | Median | Max | Std. Dev. |
| **0** | 0.161 | 0.449 | 0.428 | 1.013 | 0.135 |
| **1** | 0.137 | 0.419 | 0.394 | 1.382 | 0.164 |
| **2** | 0.157 | 0.485 | 0.489 | 1.107 | 0.164 |

| | Elongation Index [I/L] [closer to 0 means it is more elongated] | | | | |
|---|---|---|---|---|---|
| **Ballast #** | Min. | Mean | Median | Max | Std. Dev. |
| **0** | 0.246 | 0.690 | 0.699 | 1.475 | 0.158 |
| **1** | 0.357 | 0.698 | 0.686 | 2.437 | 0.210 |
| **2** | 0.029 | 0.714 | 0.727 | 1.208 | 0.165 |

| | Sphericity [closer to 1 means it is closer to a sphere / perfect block] | | | | |
|---|---|---|---|---|---|
| **Ballast #** | Min. | Mean | Median | Max | Std. Dev. |
| **0** | 0.409 | 0.668 | 0.678 | 0.922 | 0.097 |
| **1** | 0.419 | 0.653 | 0.645 | 1.499 | 0.129 |
| **2** | 0.264 | 0.691 | 0.693 | 0.990 | 0.121 |

| | Volume [inch$^3$] | | | | |
|---|---|---|---|---|---|
| **Ballast #** | Min. | Mean | Median | Max | Std. Dev. |
| **0** | 0.027 | 0.375 | 0.289 | 1.639 | 0.287 |
| **1** | 0.176 | 2.040 | 1.442 | 11.917 | 1.990 |
| **2** | 0.028 | 3.457 | 2.228 | 14.999 | 3.474 |

Comparisons of the three ballast materials show relatively similar values for the mean flatness index, elongation index, and sphericity. Of note are some outliers such as the minimum sphericity and elongation index of ballast 2 being significantly less than the minimums from the gravel or ballast 1. This implies that while the averages may be similar, there may be a distribution of sharper ballast rocks that could potentially influence the sliding behavior of a crosstie across the ballast.

## Results to Date: Compression Tests

Compression tests were conducted on crosstie materials. While dry wooden crossties are often tested in 4-point bending (see e.g., (5,6,7)) and HDPE (8,9,10) has been tested and characterized in tension, compressive properties are needed for accurately understanding how ballast rock pushes globally and locally on a crosstie. It is not believed that there is data on the local compression of a wood tie perpendicular to the grain. Further, relatively little data is known about saturated wood crossties.

The compression test samples were 2.0 inches long with square cross sections approximately 0.8 to 0.9 inches across. The compression test configuration is shown in Figure 5 and a photo of the experiment is shown in Figure 6.

The specimens included HDPE, dry wood, and wet (saturated) wood. The wood specimens were cut such that the test is generally perpendicular to the grain (i.e., the longitudinal direction of the crosstie) as shown in Figure 7.

Table 2 shows the primary results from the compression tests based on the stress-strain curves produces in Figure 8 to Figure 10. In the figures, some irregularity is observed that is a result of the loading method (i.e., slight load increases and decreases). Table 2 shows that when the wood becomes saturated with water, its elastic modulus and yield strength decrease. Test scatter is also noted in the table and stress-strain curves; the variation of the cross-grain wood angle produces a sizeable range of values from the dry and wet wood. It was difficult to get all of the grains to be perpendicular to the loading direction – in all cases the arc of the grains was roughly perpendicular. As mentioned, this cross-grain behavior and material properties are of primary interest because it is believed that this is the direction (and not the parallel-to-the-grain direction) commonly loaded by ballast rock.

**Table 2: Compression Test Results for Wood Perpendicular to the Gain and HDPE.**

| Material | E [ksi] | Yield Strength [ksi] | # of Tests |
|---|---|---|---|
| **Dry Wood** | 140 | 2.1 | 5 |
| **Wet Wood** | 79 | 1.3 | 4 |
| **HDPE** | 152 | 2.4 | 5 |

| | E [ksi] | | Yield Strength [ksi] | |
|---|---|---|---|---|
| **Material** | **Min.** | **Max.** | **Min.** | **Max.** |
| **Dry Wood** | 72 | 182 | 1.8 | 3.0 |
| **Wet Wood** | 95 | 179 | 1.0 | 1.9 |
| **HDPE** | 141 | 160 | 2.1 | 2.5 |

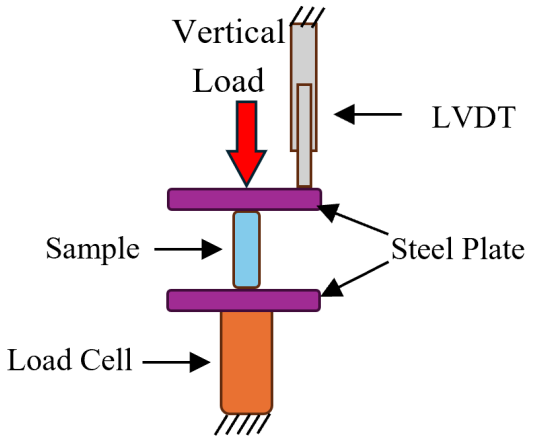


**Figure 5. Schematic of Compression Test.**

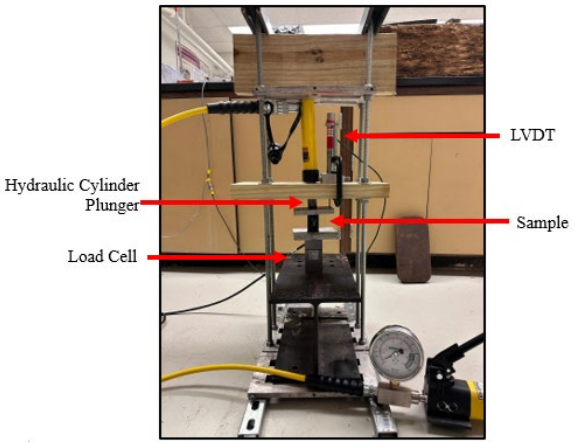


**Figure 6. Compression Test Frame with Sample.**

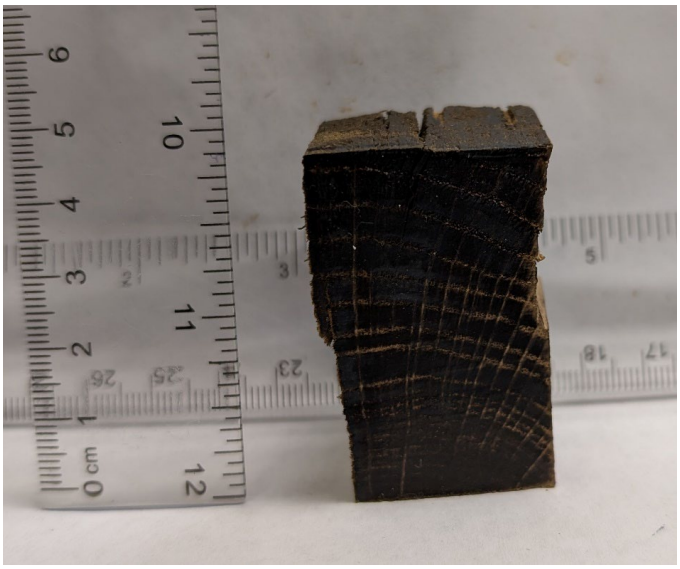

**Figure 7. Photos of Cross-Grain Wood Testing Specimens.**

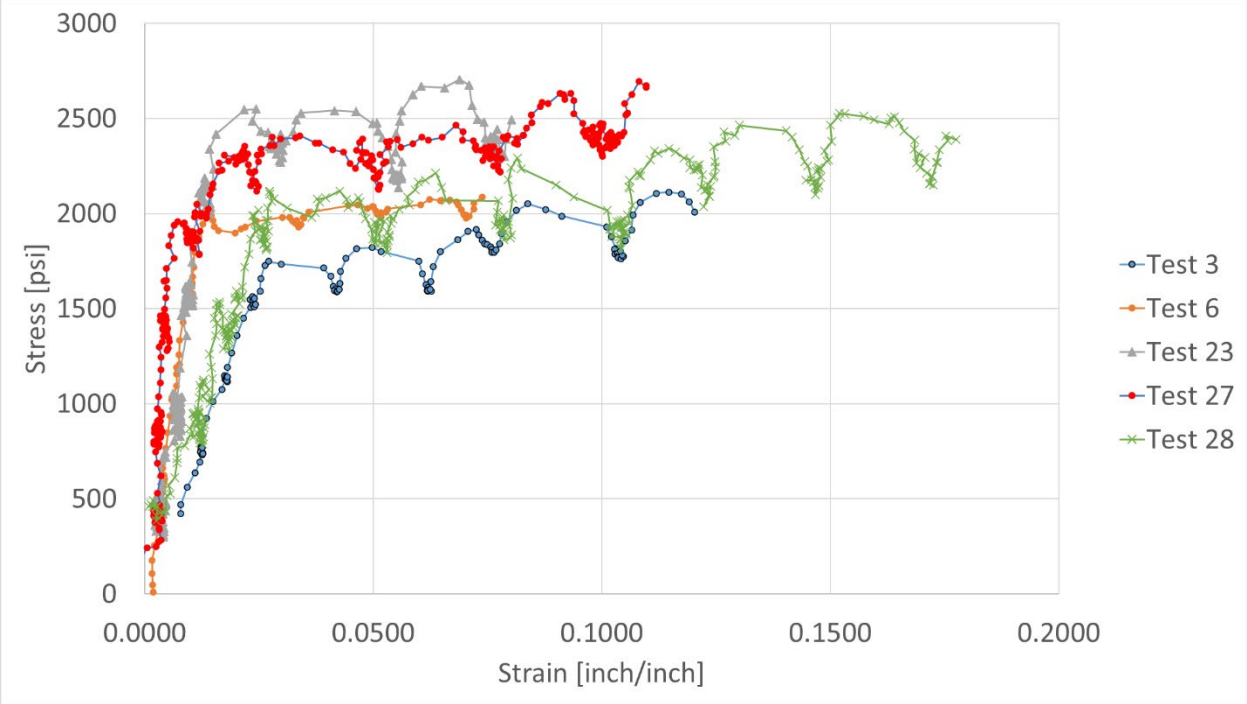


**Figure 8. Compression Test Results: Cross-Grain Dry Wood.**

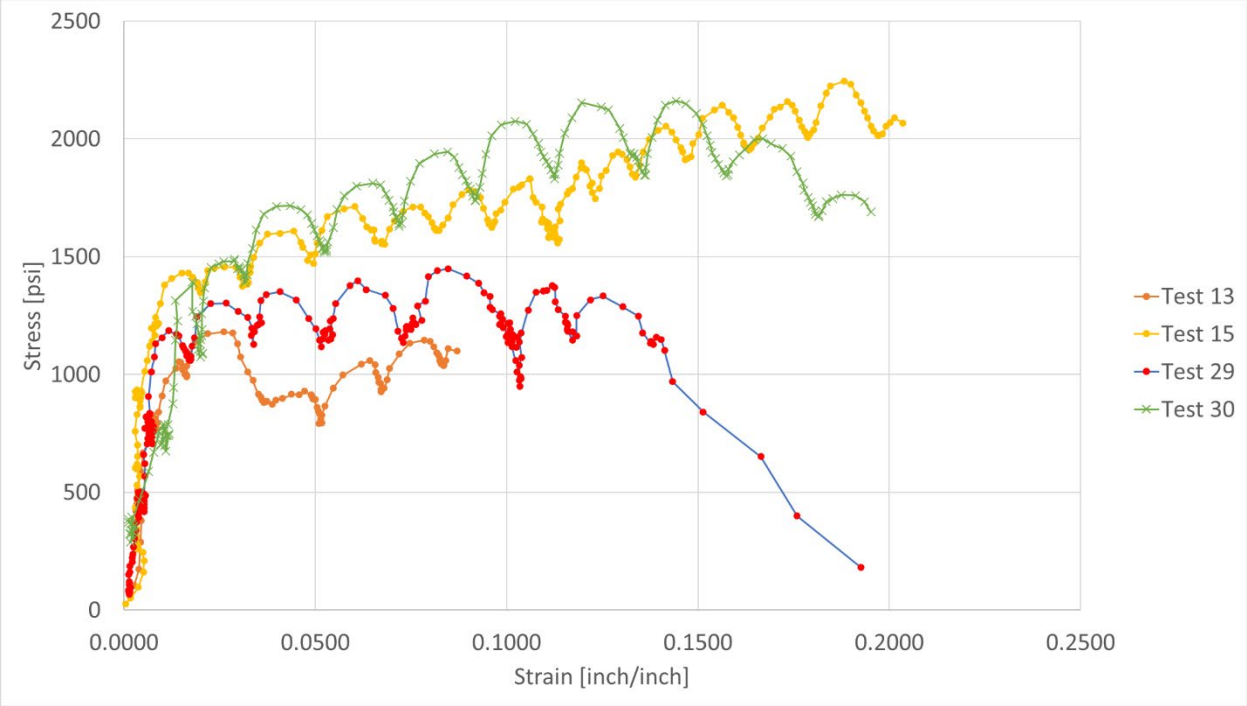


**Figure 9. Compression Test Results: Cross-Grain Wet Wood.**

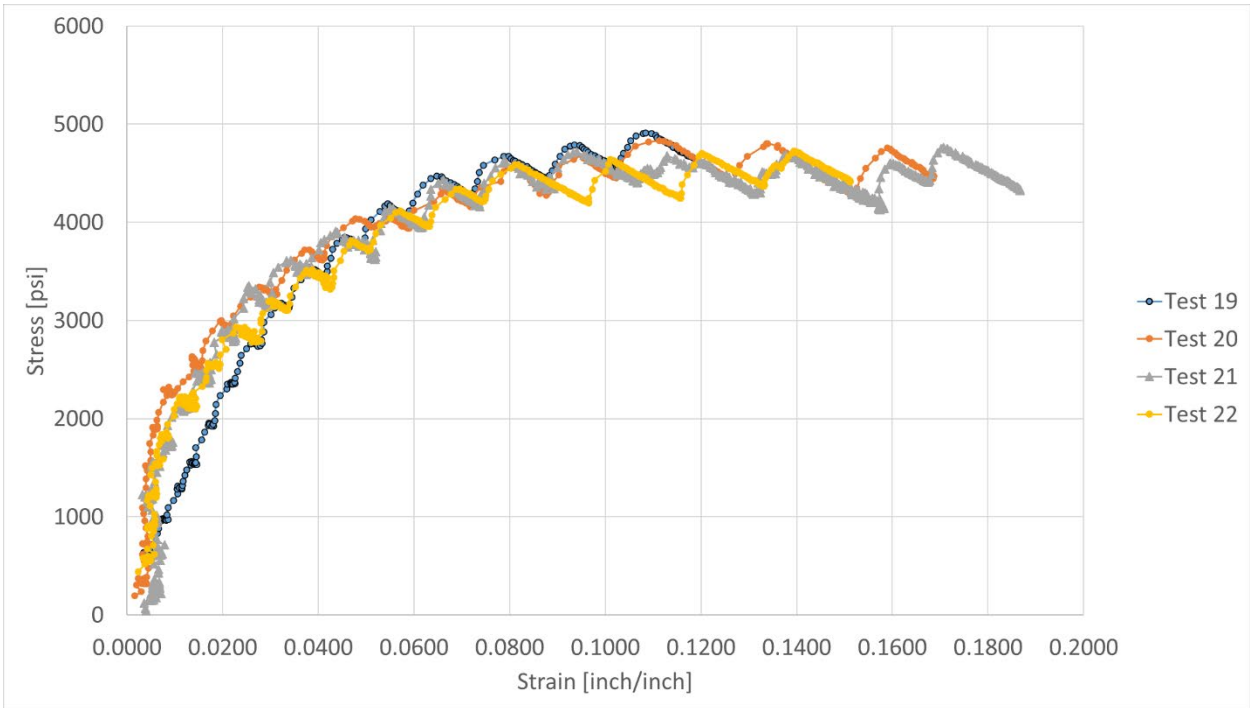


**Figure 10. Compression Test Results: HDPE.**

## Results to Date: Indentation Tests

To examine the local behavior of a single rock pushing on or penetrating into a crosstie, indentation tests were performed. These indentation tests included two diameters of steel balls (15 and 36.5 mm (0.59 and 1.44 inches)) pushed into dry wood crossties, wet (saturated) wood crossties and HDPE crossties.

The use of a steel ball to examine the indentation response is often performed in hardness tests on a wide variety of materials such as plastics and metals, with steel hardness tests being common for quality checks on a wide variety of alloys. The Janka hardness test is a documented tests where a 15 mm steel ball is pressed into a wooden surface to examine the softness or impact resistance of woods, typically for the flooring industry.

The impact test setup included an LVDT to measure displacement and a load cell to measure applied force (see Figure 11 and Figure 12). During the test, the ball is hydraulically pressed into the tie surface. A series of crosstie tests were performed: dry wood, wet (saturated) wood, and HDPE crossties. Two indentation ball diameters were used: 15 mm and 36.5 mm. The ball was pressed into the crosstie until a load of approximately 3150 lbs (14 kN) was obtained.

Table 3 and Table 4 show the results gathered from the indentation tests using the 15 mm and 36.5 mm diameter balls, respectively. Photos of the indentations left in the wood and HDPE crossties are shown in Figure 13 and Figure 14.

As noted from the compression tests, the relatively large wood grains create a scatter in the indentation results that is not as significant in the HDPE results. Further, the wet wood indentation is deeper for the 15 mm ball as compared to the dry wood. However, for the larger diameter, 36.5 mm, ball, the reverse is shown: the dry wood indentation is deeper than the wet wood. This is believed to be a function of the scatter from the indenter's location relative to wood grains. More testing may reveal a better distribution where the wet wood indentions are expected to average deeper than the dry wood indentions.

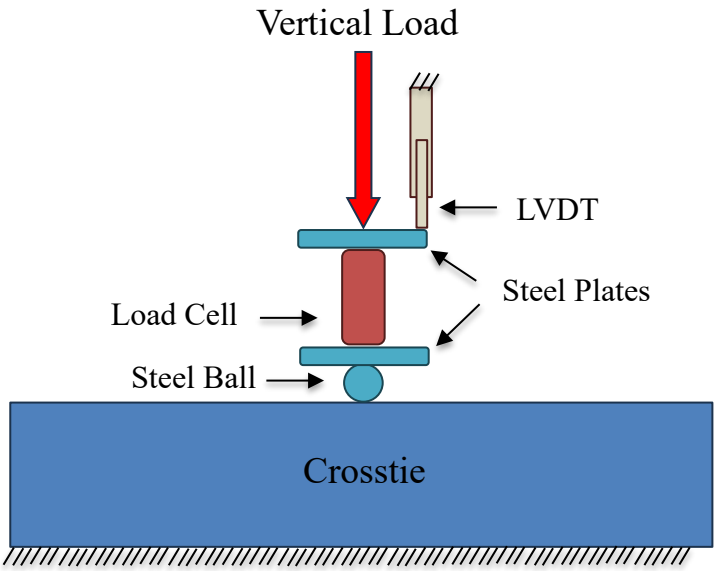


**Figure 11. Schematic of Indentation Test.**

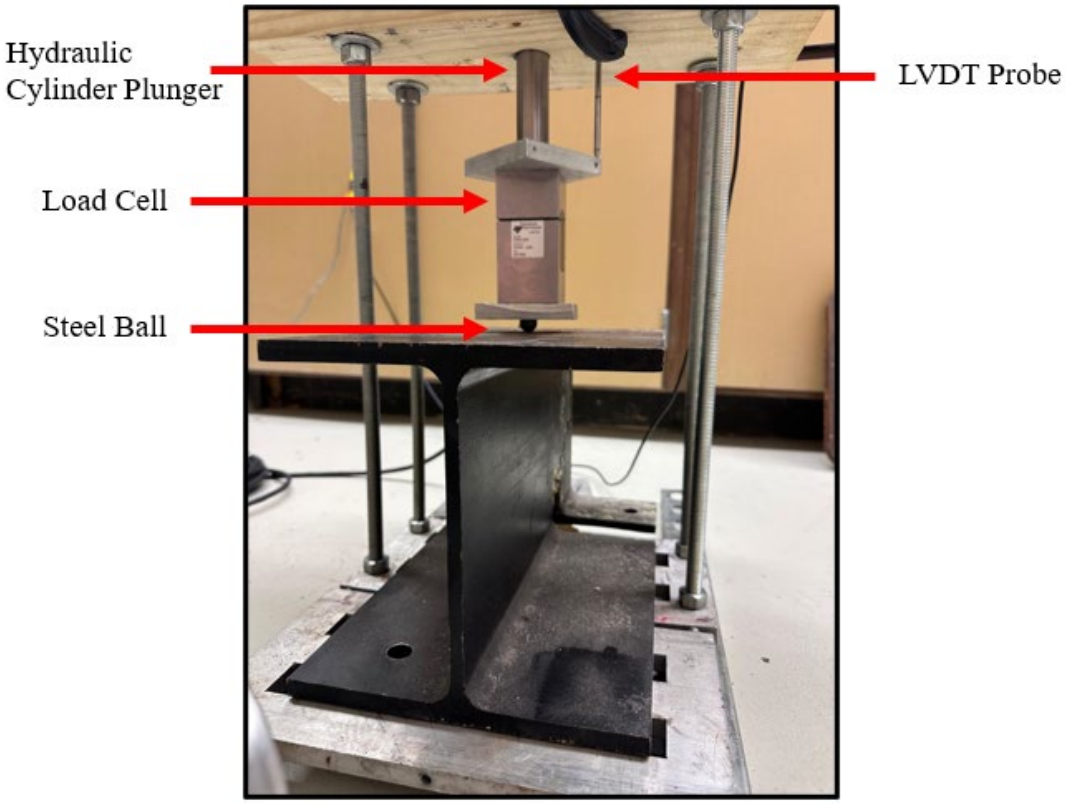


**Figure 12. Indentation Test Setup.**

**Table 3: Indentation Results: 15 mm Ball loaded to ~3150 lbs.**

| Tie Material | # of Tests | Mean Indention Depth [inch] | Std. Dev. Indention Depth [inch] |
|---|---|---|---|
| Dry Wood | 12 | 0.29 | 0.05 |
| Wet Wood | 10 | 0.32 | 0.06 |
| HDPE | 9 | 0.25 | 0.02 |

**Table 4: Indentation Results: 36.5 mm Ball loaded to ~3150 lbs.**

| Tie Material | # of Samples | Mean Indention Depth [inch] | Std. Dev. Indention Depth [inch] |
|---|---|---|---|
| Dry Wood | 6 | 0.18 | 0.04 |
| Wet Wood | 5 | 0.18 | 0.05 |
| HDPE | 6 | 0.12 | 0.02 |


**Figure 13. Post-Test Indentation from 15 mm Ball on Dry Wooden Tie.**


**Figure 14. Post-Test Indentation from 15 mm Ball on HDPE Tie.**

**Results to Date: FEA of Single Point Indentation and Sliding Friction**

Because of the importance of compression and indentation behavior in different crossties, finite element models were used to validate the material properties. The compressive material properties were used in the finite element model to verify the indentation vs force relationship displayed in the indentation tests. Separate models were used to evaluate the sequence of:

A. An indentation (e.g., from a single ballast rock) pushing into the crosstie material.
B. The indentation then laterally moving at the indentation depth.

The purpose of this second model was to examine the effective lateral friction of a single rock.

***Axisymmetric Indentation Model***

A 2D axisymmetric model simulating the indention test was developed in the general-purpose finite element software ANSYS. The model included a elastic steel ball and elastic-plastic crosstie material response. Both the 15 mm and 36.5 mm diameter balls were modeled. Crosstie properties were prescribed based on the compression test results for dry wood, wet wood, and HDPE. Other modeling details included large deformation theory, 2$^{nd}$ order elements, and implicit formulation. Model variations included changing the coefficient of friction from 0.10 to 0.25 to 0.50.

The model geometry is shown in Figure 15. The meshes are shown in Figure 16, the 15 mm diameter ball model had 3400 elements (8800 nodes) and the 36.5 mm diameter ball model had 17,000 elements (43000 nodes). The right and bottom surfaces were fixed and the horizontal top of the ball was displaced down.

Results are shown in Figure 17 and Figure 18 for the 15 mm and 36.5 mm diameter balls. Results are presented in those figures showing the equivalent plastic strain accumulation beneath the indentation. The load-displacement results for the dry wood, wet wood, and HDPE are shown in Figure 19 to Figure 24.

The purpose and importance of this simulation was to both verify the compressive behavior of the crosstie and to estimate the coefficient of friction. The compressive properties of the crossties were specified from the compression tests noting that the scatter on the elastic modulus and yield strength is inherently high for the small number of samples (and, as mentioned, is partly a result of the grain size and cross-grain angles in that test). In the FE result graphs in Figure 19 to Figure 24, the red dot indicates the average depth from an indentation load of 3150 lbs (14 kN).

Main takeaways:

a. For the 36.5 mm diameter ball indention simulations, friction doesn't influence the FE results. The indenter pushes in such a shallow amount that there is negligible relative sliding between the indenter and the base material (i.e., crosstie).
b. From the dry wood results, it appears that either the elastic modulus of the dry wood (from the compression tests) is slightly (~20%) high or the indentation test results are slightly less deep than expected. More testing (both compression and indentation) is recommended.
c. For the wet wood results, it appears that either the elastic modulus of the wet wood (from the compression tests) is slightly (~10%) low for the 15 mm diameter ball. However, the 36.5 mm diameter ball agrees very well between the indentation result and the FE result.
d. The HDPE results are in good agreement for both the 15 and 36.5 mm diameter balls.

Further work could also include the scatter on the data to provide confidence bands for these results.

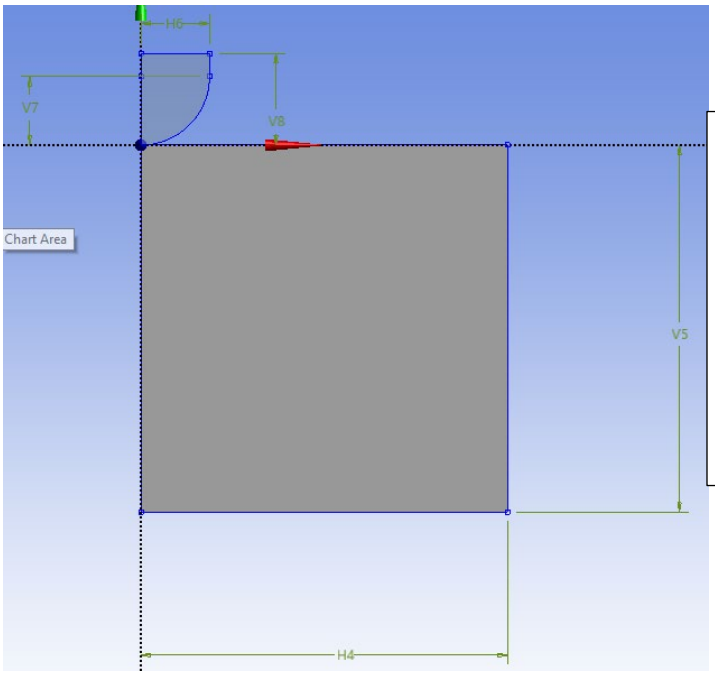


General Geometry:

15 mm ball: 40 mm x 40 mm block (0.59 inch ball on 1.57x1.57” block)

36.5 mm ball: 80 mm x 80 mm block (1.44 inch ball on 3.15x3.15” block)

**Figure 15. Axisymmetric Indention Model Geometry.**

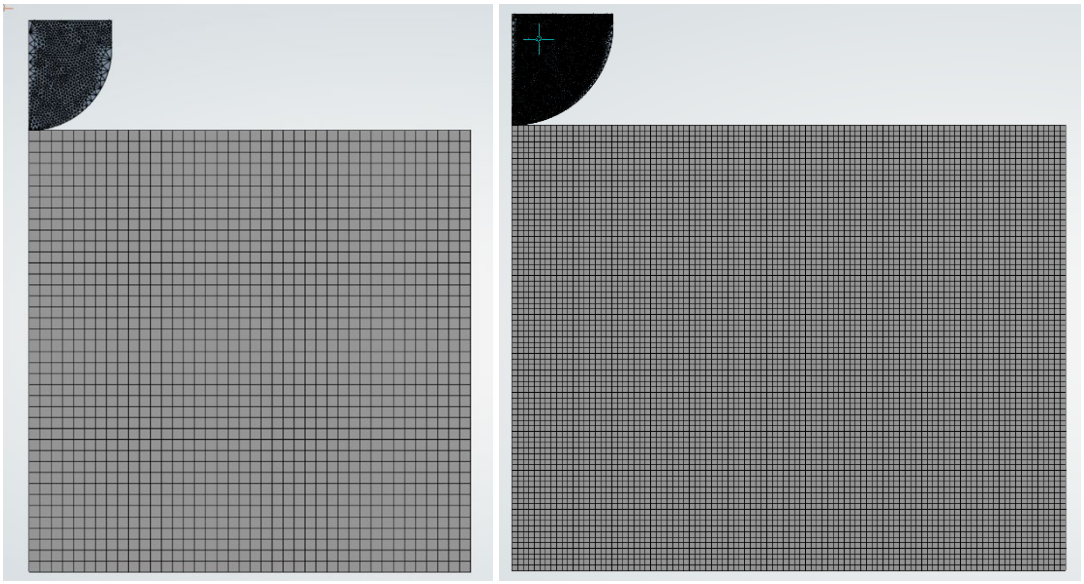

15 mm diameter ball | 36.5 mm diameter ball

**Figure 16. Axisymmetric Indentation Meshes.**

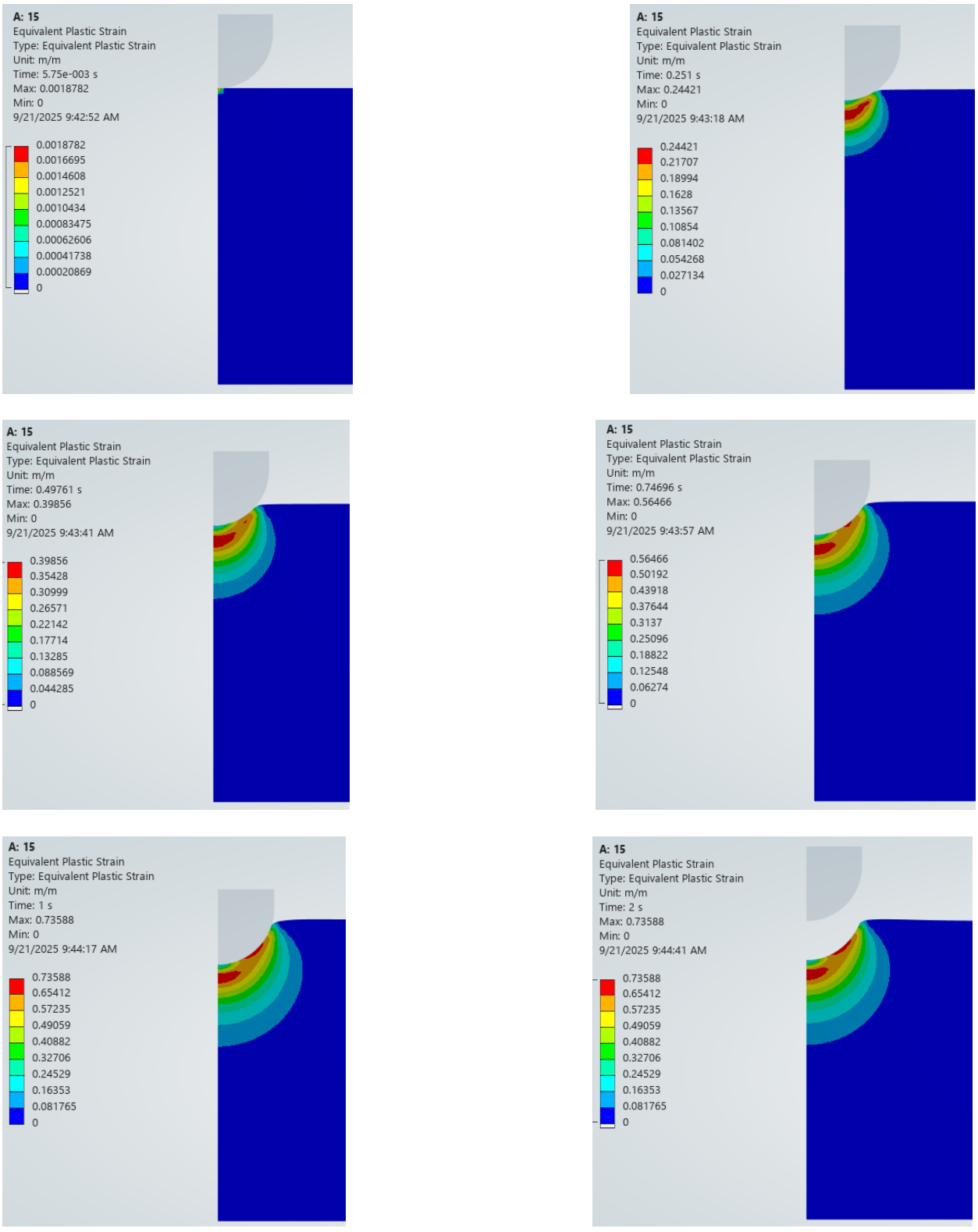


**Figure 17. Exemplar Indentation Results for 15 mm Ball: Equivalent Plastic Strain.**

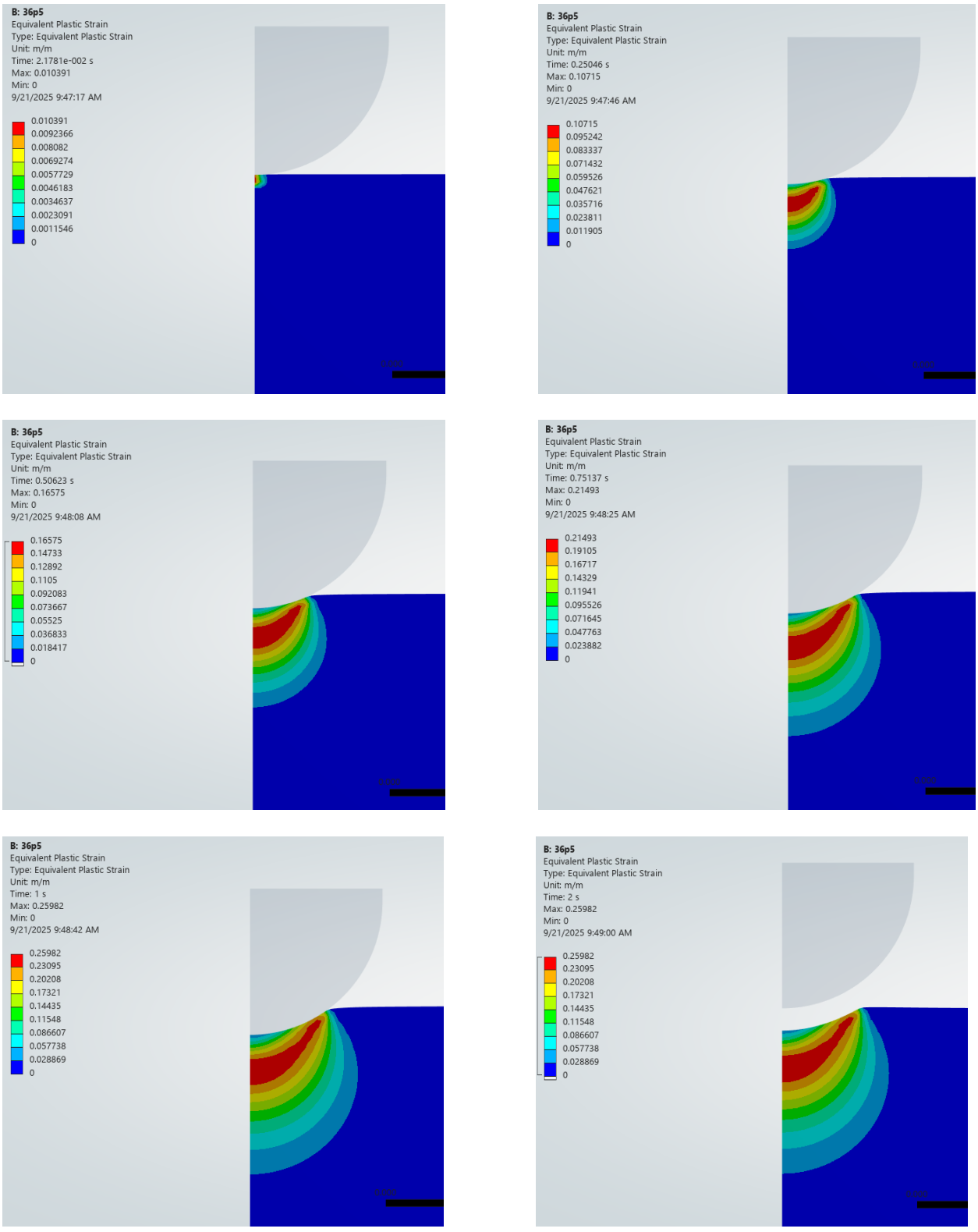


**Figure 18. Exemplar Indentation Results for 36.5 mm Ball: Equivalent Plastic Strain.**

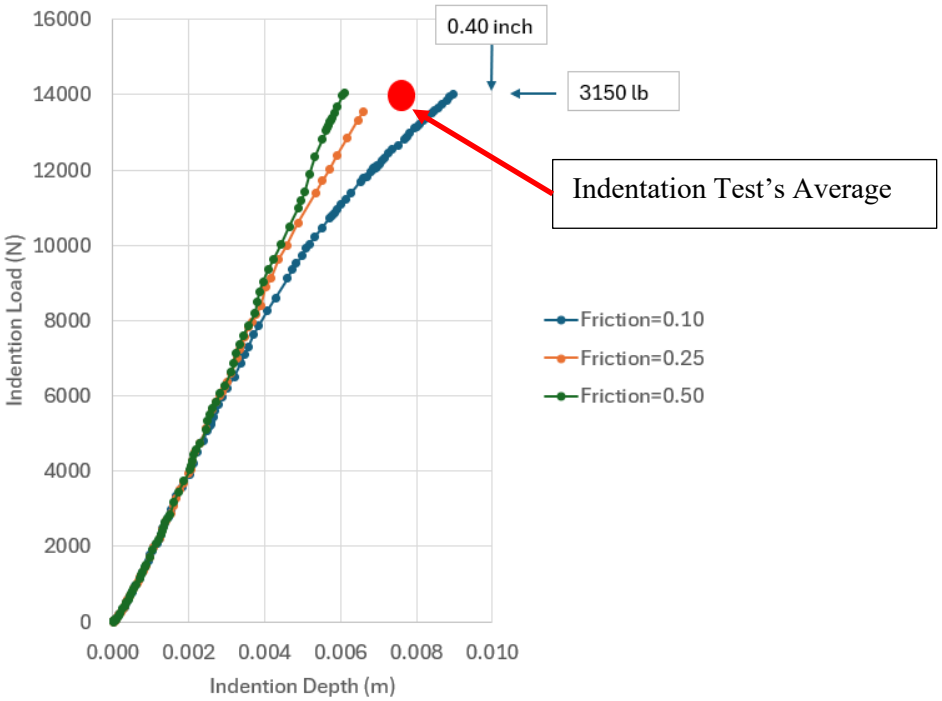


**Figure 19. Axisymmetric Results: Dry Wood, 15 mm Ball.**

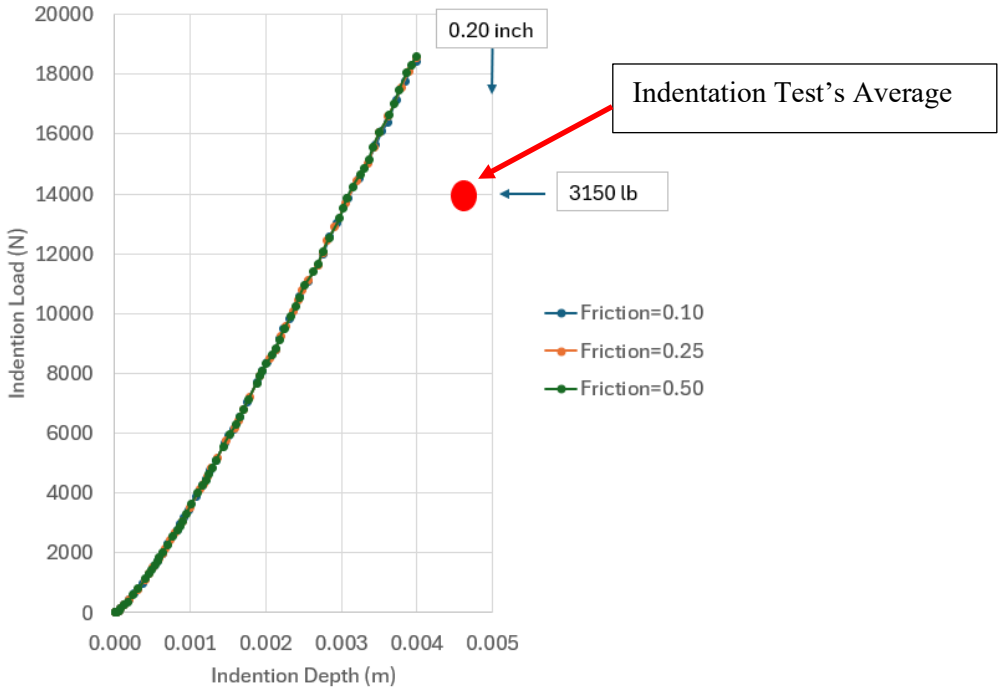


**Figure 20. Axisymmetric Results: Dry Wood, 36.5 mm Ball.**

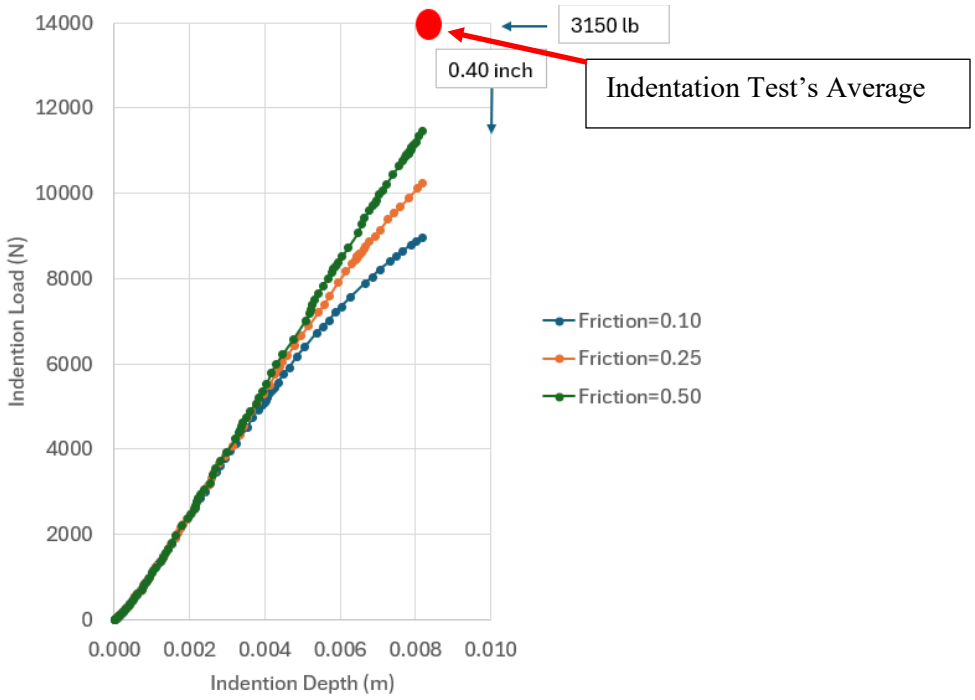


**Figure 21. Axisymmetric Results: Wet Wood, 15 mm Ball.**

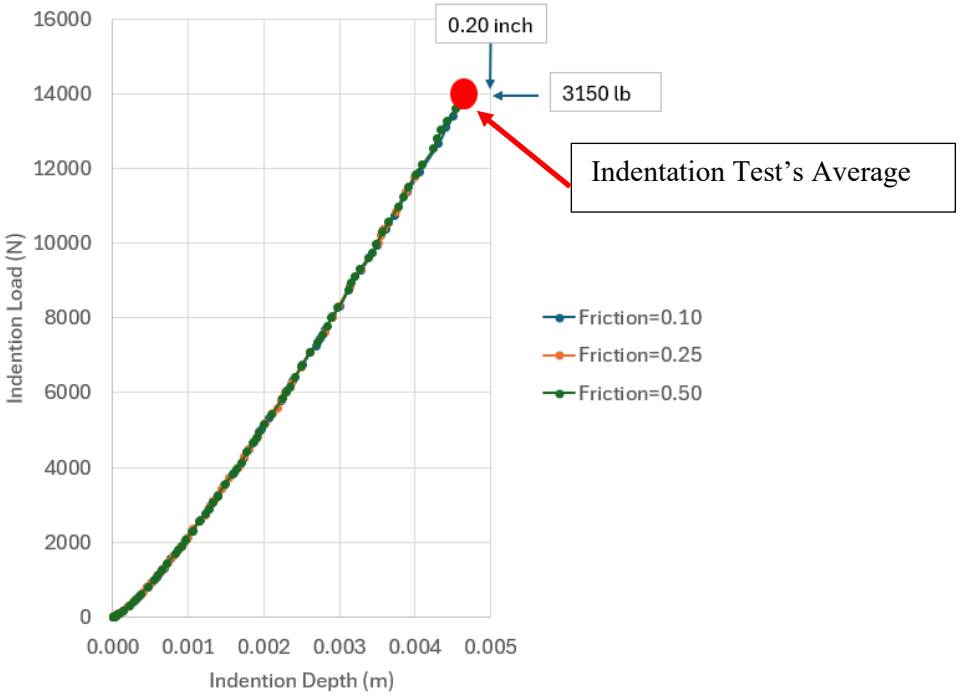


**Figure 22. Axisymmetric Results: Wet Wood, 36.5 mm Ball.**

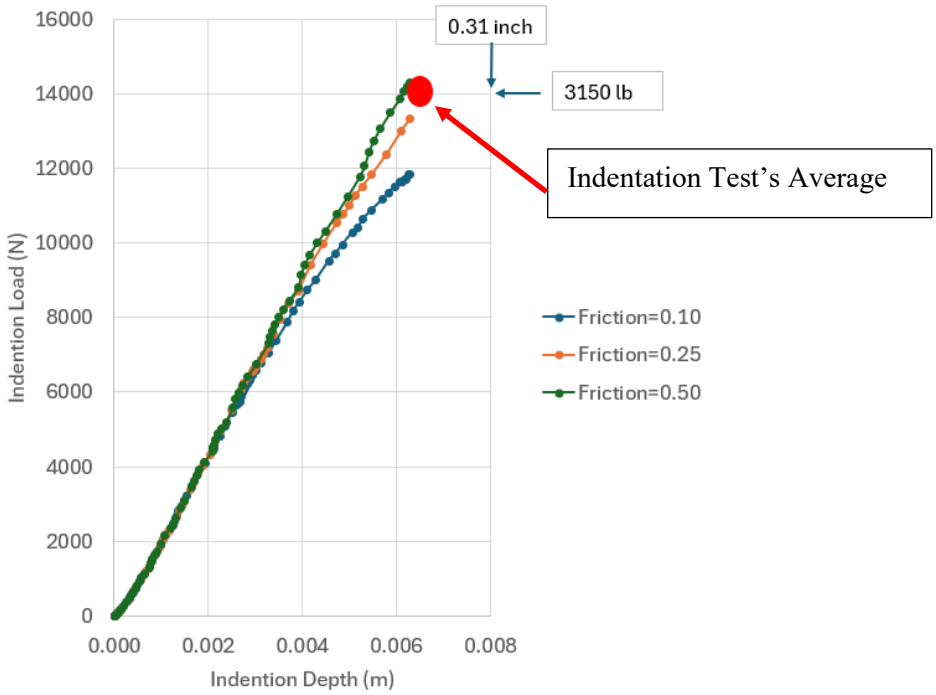


**Figure 23. Axisymmetric Results: HDPE, 15 mm Ball.**

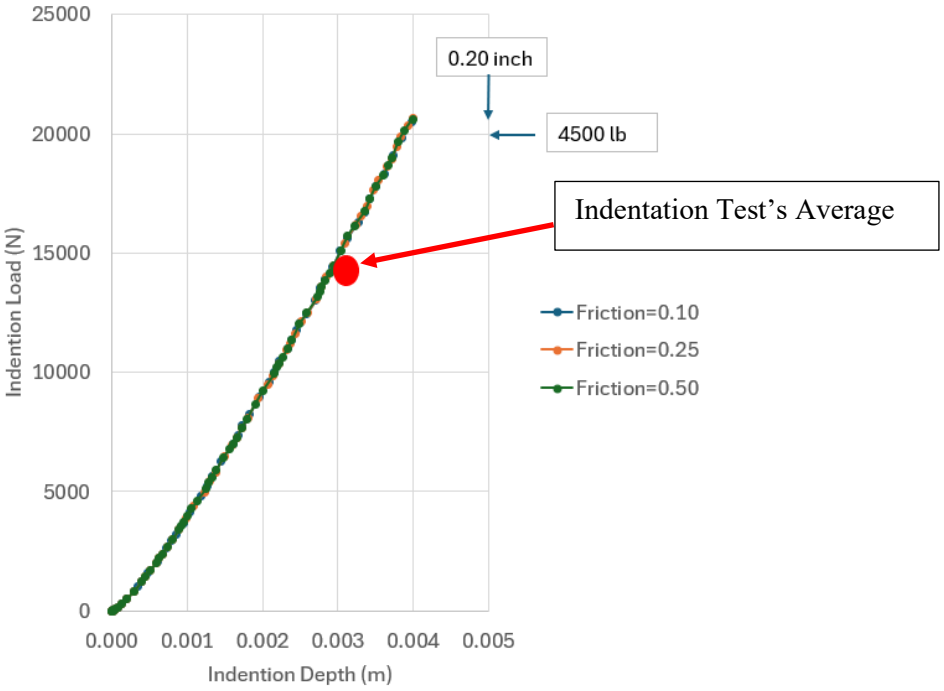


**Figure 24. Axisymmetric Results: HDPE, 36.5 mm Ball.**

***Half-Symmetry Model for Indentation and Lateral Movement***

A finite element model was created to simulate a single ballast rock indenting into a crosstie and then displacing laterally. The goal of this model was to understand the frictional resistance for different indenter diameters (i.e., simulating different rock diameters or facets) at different indent depths.

A half-symmetry model was created with indenter diameters of 15 mm and 36.5 mm (to carry on the indenter diameters in the indention experiments and other finite element work). An image of the geometry is shown in Figure 25 and an image of the mesh is shown in Figure 26. The model had 59,000 second order elements and 125,000 nodes. The run included an elastic steel indenter and elastic-plastic block (crosstie) response with large deformation theory and an implicit solution.

The block (crosstie) bottom was held fixed. The indenter was displaced into the block (-Y direction) distances of 1.0, 5.0 and 7.5 mm (0.039, 0.197, and 0.295 inches). The indenter was then displaced laterally 10 mm (0.39 inches).

Example results are shown in Figure 27. Graphs of the lateral load as a function of the lateral sliding distance are shown in Figure 28 and Figure 29. As shown in the graphs, the indentation depth of a rock into a crosstie can create a rapid increase in the lateral force required to move the rock relative to the crosstie. The distance required to get to a steady-state resistance depends on the indentation depth and indentation diameter.

The effect of interfacial friction, which wasn't significant in the finite element models of the indenter, is significant when the indenter is moved laterally: The difference between a coefficient of friction of 0.25 and 0.50 is a factor of ~2 for small indentation depths and that increase continues if the coefficient of friction goes to 0.75.

The prime takeaway from these trends is the significant lateral resistance from deep indents and high friction. The deeper indents are a function of the facetedness of the ballast rock and, as discussed in the next section, the number of indents over the crosstie surface area.

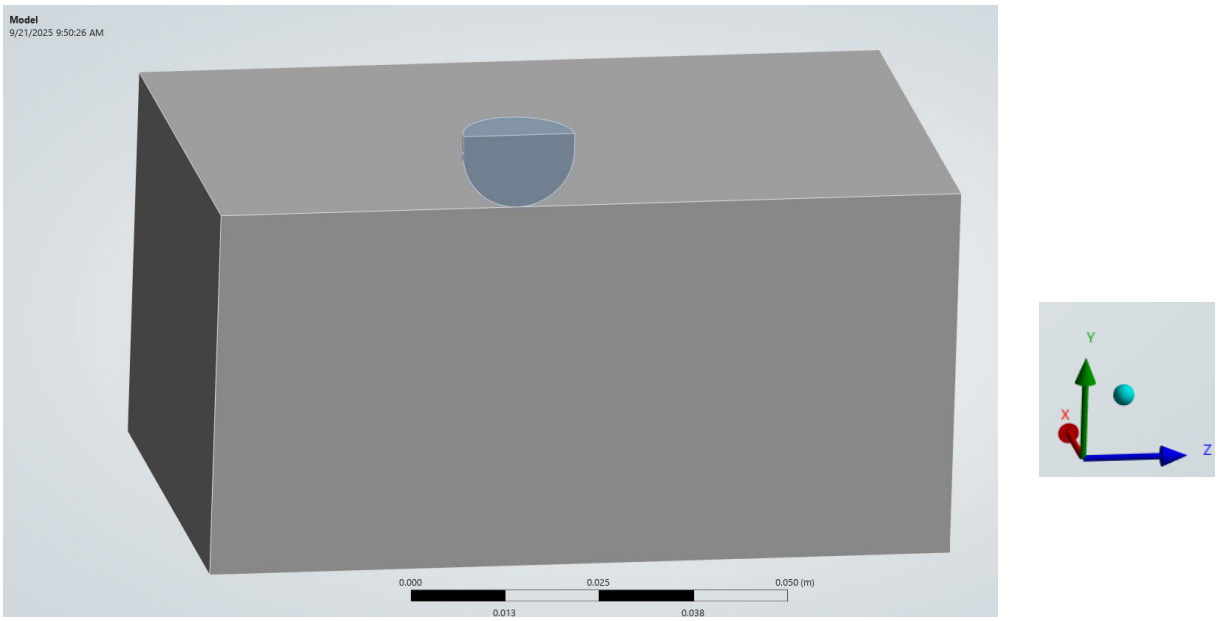


**Figure 25. Half-symmetry Model of Indenter.**

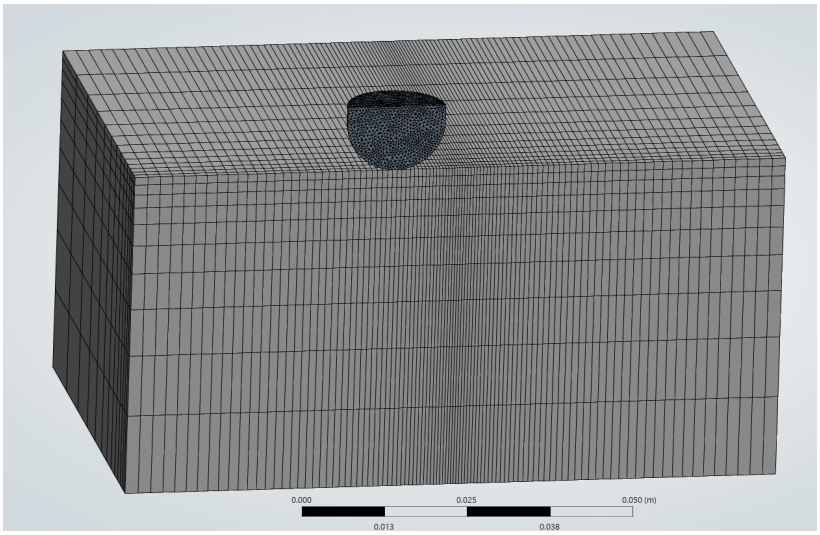


**Figure 26. Half-symmetry Model of Indenter: Mesh.**

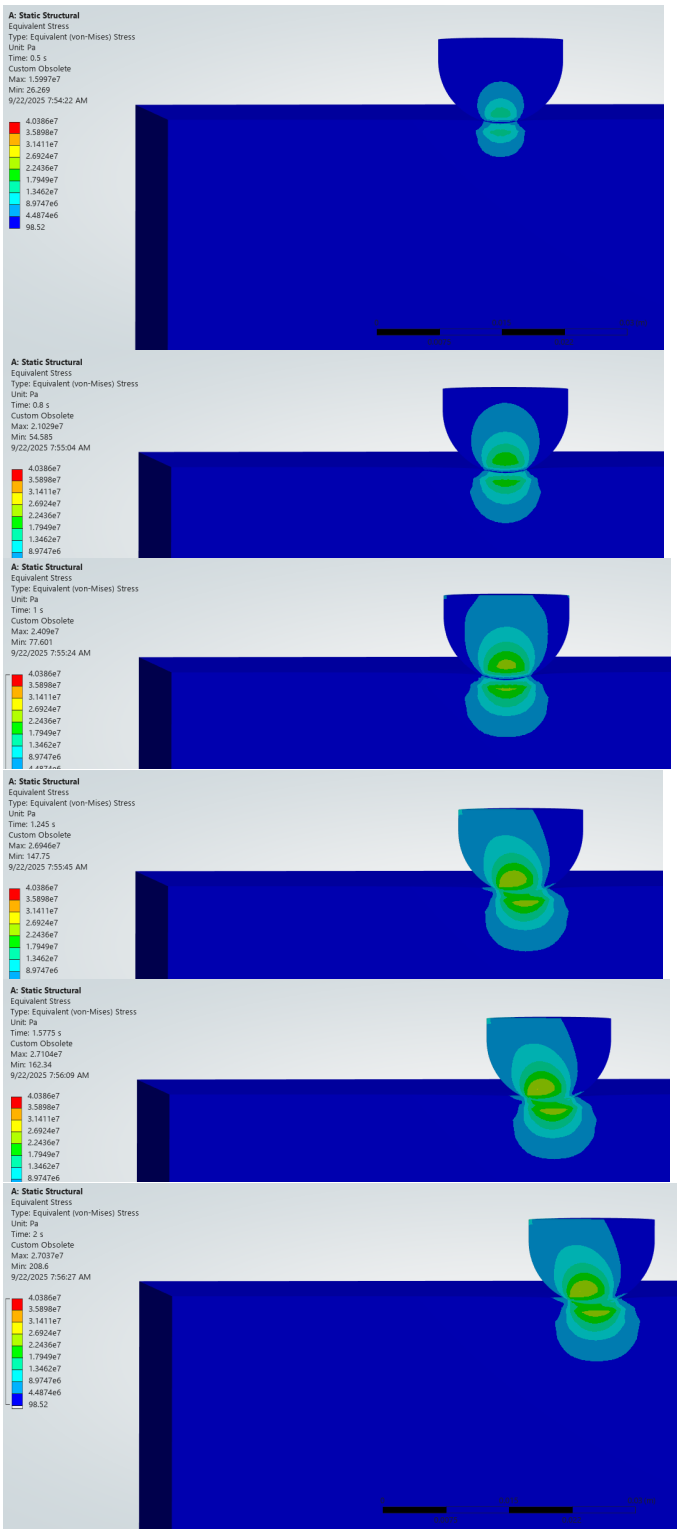


**Figure 27. Half-symmetry Model of Indenter: Example Results.**

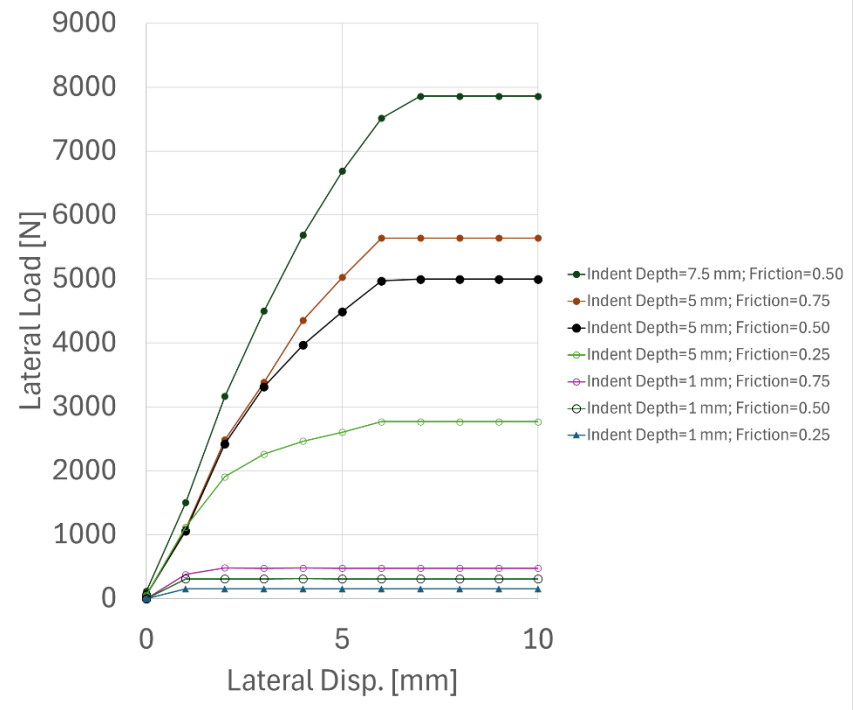


**Figure 28. Finite Element Indentation and then Sliding Results: 15 mm Diameter Indenter.**

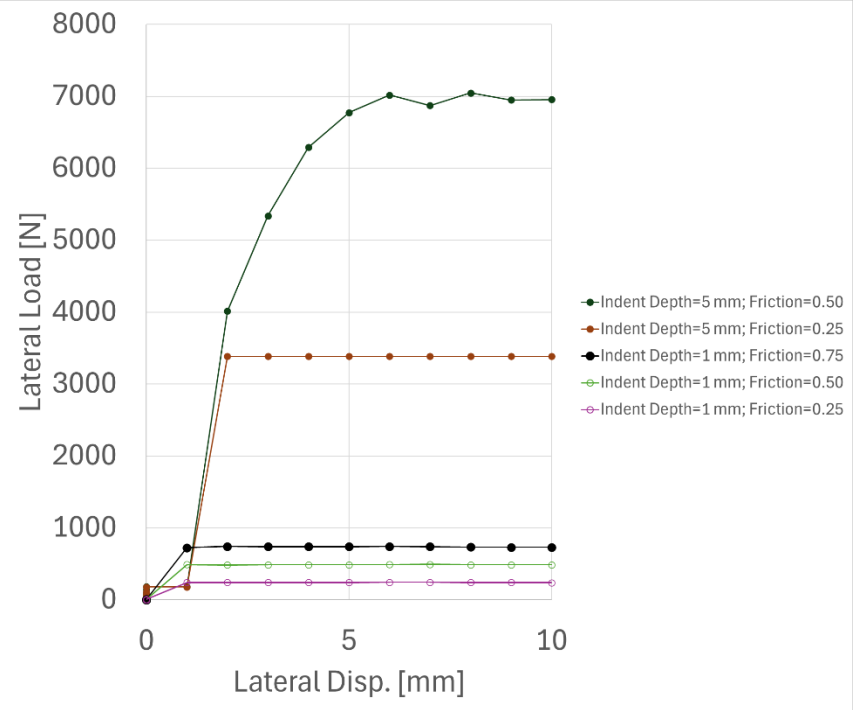


**Figure 29. Finite Element Indentation and then Sliding Results: 36.5 mm Diameter Indenter.**

## Results to Date: Ballast Indentation Data

To characterize how each ballast type interacts with the face of the crosstie, a 12x8x2 inch piece of polystyrene foam was placed onto the bed of ballast with 250lbs of weight placed on top. This procedure created a type of topographical map of the surface of the ballast surface when a crosstie is placed on top (see Figure 30). The minimum and maximum diameter between the edges of the holes as well as the max depth were recorded to calculate the damaged area, average depth of the indents, and number of contact points on the polystyrene foam face.

Each indentation was modeled using the measured minimum and maximum rim diameters $d_{min}$ and $d_{max}$ and the maximum depth, $h$. The damaged plane area for each crater was calculated using the elliptical circle formula:

$$A = \frac{\pi}{4} * d_{min} * d_{max}$$

Figure 31 denotes four unique indentions where the surface of the polystyrene foam has been displaced due to the peaks and edges of the ballast surface.

Table 5 shows the average indent density, percent area damaged and the average depth of each indentation recorded on the piece of polystyrene foam. The indent density column shows the average distance between each damaged section, a higher number means a more spread pattern across the sample. Ballast 0 (common gravel) had the densest indent per square inch ratio compared to the other ballast types. Given that ballast type 0 distributes the load much more uniformly compared to the other ballasts, the average depth for each indention was considerably lower than the other two types by as much as 0.040 inches.

Ballast type 2 had more jagged and elongated rocks compared to the other ballast types leading to less interlocking and greater variation in the interface between the sample and rocks. The full data collection is shown in Table 6.

A key takeaway from this is that the ballast with the larger size typically produces fewer indents over an area- with those indents being deeper. These deeper indents will have a significantly greater resistance to lateral movement as discussed in the section covering the finite element modeling of the indent followed by the lateral movement. Finally, the sharpness of the ballast is important here: sharper ballast has an increased likelihood of penetrating deeper into the crosstie and anchoring it or resisting lateral forces to a greater extent than shallower indents from ballast rock.

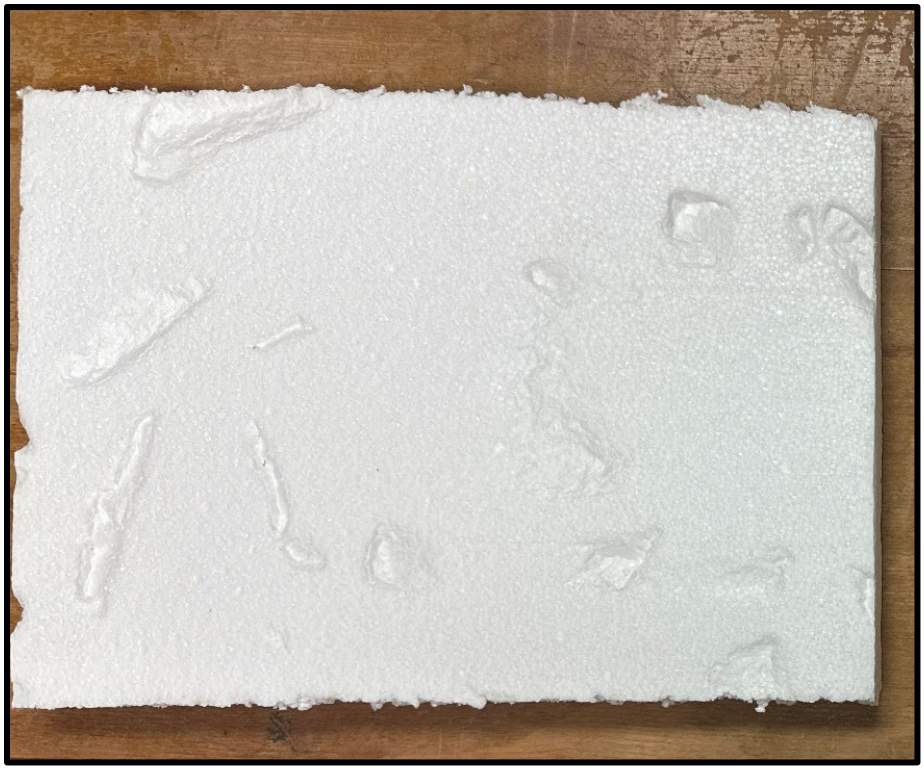

**Figure 30. Polystyrene Foam Piece after being Pressed into Ballast Bed.**

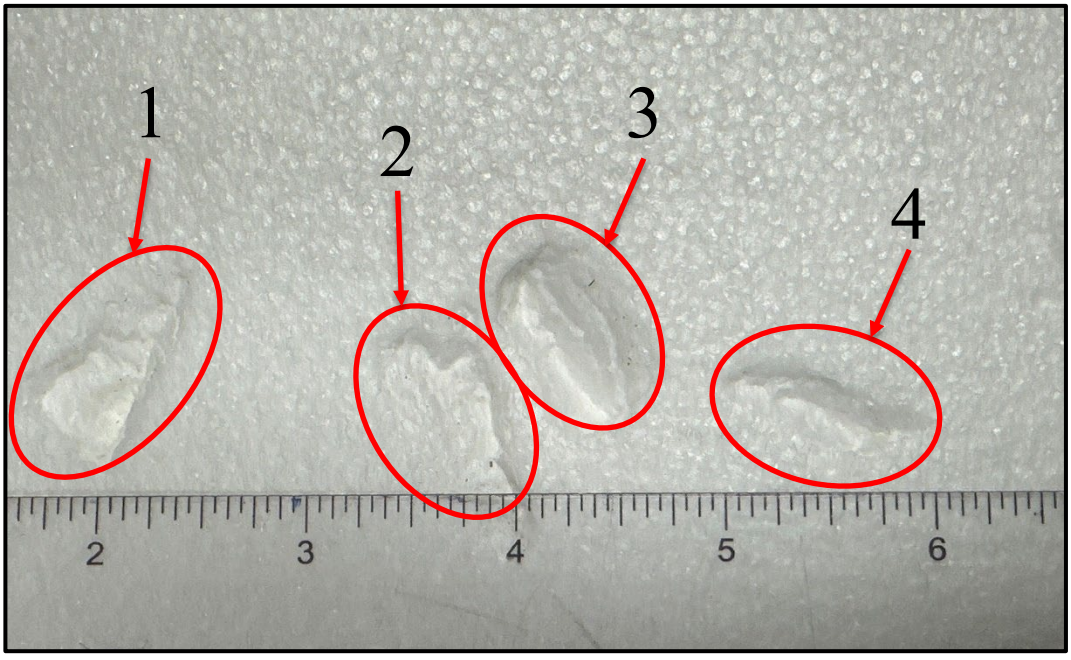


**Figure 31. Remaining Indentations from Ballast 1.**

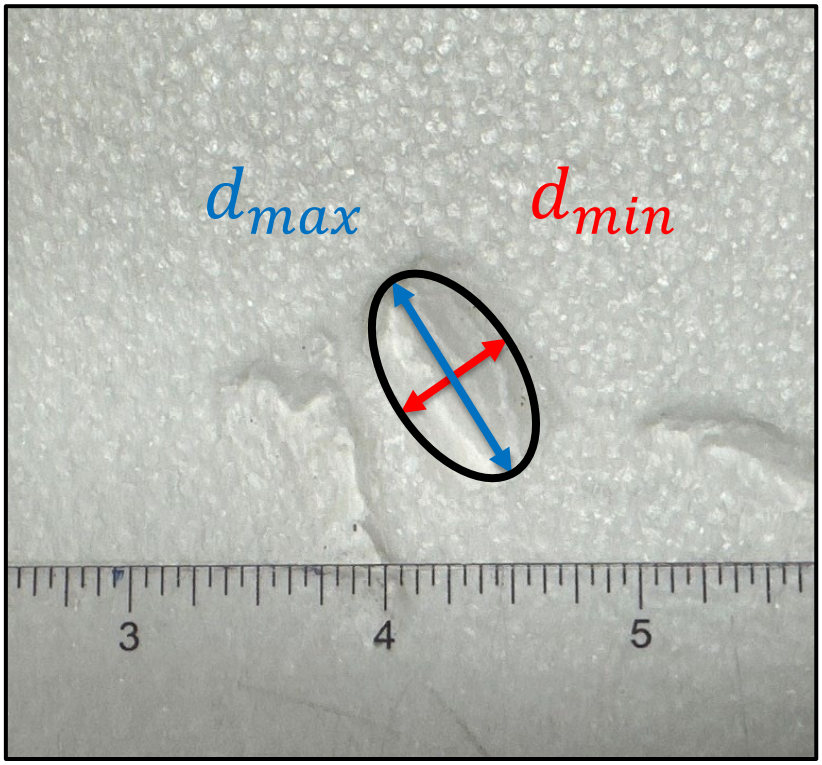


**Figure 32. Indention Measurements.**

**Table 5: Ballast Characteristics using Press Test.**

| Ballast # | Indent Density [inch$^2$/Number] | Area Damaged [%] | Avg. Depth [inch] |
|---|---|---|---|
| 0 | 2.11 | 7.37 | 0.07 |
| 1 | 4.38 | 8.57 | 0.13 |
| 2 | 5.95 | 12.28 | 0.11 |

**Table 6: Indentation Data.**

| Ballast # | Sample Piece | Indent # | Min Diamter [inch] | Max Diameter [inch] | Depth [inch] |
|---|---|---|---|---|---|
| 2 | 2 | 1 | 0.402 | 0.347 | 0.06 |
| 2 | 2 | 2 | 1.112 | 2.545 | 0.196 |
| 2 | 2 | 3 | 0.158 | 0.711 | 0.065 |
| 2 | 2 | 4 | 0.182 | 0.467 | 0.049 |
| 2 | 2 | 5 | 0.674 | 1.415 | 0.278 |
| 2 | 2 | 6 | 0.753 | 0.977 | 0.28 |
| 2 | 2 | 7 | 1.21 | 2.441 | 0.154 |
| 2 | 2 | 8 | 0.44 | 0.822 | 0.068 |
| 2 | 2 | 9 | 0.15 | 0.436 | 0.081 |
| 2 | 2 | 10 | 0.138 | 0.688 | 0.039 |
| 2 | 2 | 11 | 0.087 | 0.355 | 0.015 |
| 2 | 2 | 12 | 0.657 | 0.819 | 0.203 |
| 2 | 2 | 13 | 0.26 | 0.406 | 0.083 |
| 2 | 2 | 14 | 0.081 | 0.31 | 0.04 |
| 2 | 2 | 15 | 0.527 | 1.281 | 0.091 |
| 2 | 2 | 16 | 0.707 | 1.809 | 0.085 |
| 2 | 2 | 17 | 1.321 | 1.396 | 0.128 |
| 2 | 2 | 18 | 1.591 | 0.919 | 0.135 |
| 2 | 2 | 19 | 0.471 | 0.924 | 0.152 |
| 2 | 2 | 20 | 0.379 | 1.563 | 0.199 |
| 2 | 3 | 1 | 0.355 | 0.838 | 0.089 |
| 2 | 3 | 2 | 0.953 | 1.532 | 0.153 |
| 2 | 3 | 3 | 1.557 | 1.237 | 0.064 |
| 2 | 3 | 4 | 0.806 | 1.125 | 0.119 |
| 2 | 3 | 5 | 1.288 | 1.839 | 0.131 |
| 2 | 3 | 6 | 0.478 | 0.828 | 0.133 |
| 2 | 3 | 7 | 1.007 | 1.194 | 0.286 |
| 2 | 3 | 8 | 0.942 | 1.077 | 0.173 |
| 2 | 3 | 9 | 0.232 | 0.302 | 0.054 |
| 2 | 3 | 10 | 0.429 | 0.705 | 0.111 |
| 2 | 3 | 11 | 0.279 | 1.584 | 0.13 |
| 2 | 3 | 12 | 0.216 | 0.803 | 0.1 |
| 2 | 3 | 13 | 0.681 | 2.529 | 0.149 |
| 2 | 3 | 14 | 0.601 | 2.598 | 0.166 |
| 2 | 3 | 15 | 0.902 | 3.042 | 0.217 |
| 1 | 2 | 1 | 0.162 | 0.488 | 0.024 |
| 1 | 2 | 2 | 0.277 | 0.479 | 0.067 |
| 1 | 2 | 3 | 0.263 | 0.711 | 0.137 |
| 1 | 2 | 4 | 0.332 | 2.212 | 0.14 |

| | | | | | |
|---|---|---|---|---|---|
| 1 | 2 | 5 | 0.416 | 0.865 | 0.126 |
| 1 | 2 | 6 | 0.208 | 0.483 | 0.055 |
| 1 | 2 | 7 | 0.175 | 1.026 | 0.12 |
| 1 | 2 | 8 | 0.385 | 1.619 | 0.18 |
| 1 | 2 | 9 | 0.528 | 0.921 | 0.113 |
| 1 | 2 | 10 | 0.383 | 0.757 | 0.111 |
| 1 | 2 | 11 | 0.177 | 1.503 | 0.127 |
| 1 | 2 | 12 | 0.21 | 0.385 | 0.087 |
| 1 | 2 | 13 | 0.344 | 0.828 | 0.145 |
| 1 | 2 | 14 | 0.276 | 0.554 | 0.065 |
| 1 | 2 | 15 | 0.355 | 0.797 | 0.106 |
| 1 | 2 | 16 | 0.354 | 1.55 | 0.11 |
| 1 | 2 | 17 | 0.352 | 1.822 | 0.066 |
| 1 | 2 | 18 | 0.33 | 0.502 | 0.133 |
| 1 | 2 | 19 | 0.2 | 0.373 | 0.07 |
| 1 | 2 | 20 | 0.405 | 0.962 | 0.178 |
| 1 | 2 | 21 | 0.301 | 0.856 | 0.128 |
| 1 | 2 | 22 | 0.661 | 1.84 | 0.156 |
| 1 | 2 | 23 | 0.304 | 0.428 | 0.042 |
| 1 | 2 | 24 | 0.449 | 0.844 | 0.09 |
| 1 | 2 | 25 | 0.454 | 0.93 | 0.212 |
| 1 | 2 | 26 | 0.208 | 1.444 | 0.206 |
| 1 | 2 | 27 | 0.156 | 0.955 | 0.064 |
| 1 | 2 | 28 | 0.253 | 0.69 | 0.123 |
| 1 | 2 | 29 | 0.227 | 1.471 | 0.201 |
| 1 | 2 | 30 | 0.483 | 1.051 | 0.062 |
| 1 | 1 | 1 | 0.522 | 0.936 | 0.044 |
| 1 | 1 | 2 | 0.532 | 1.32 | 1.17 |
| 1 | 1 | 3 | 1.097 | 1.591 | 0.085 |
| 1 | 1 | 4 | 0.489 | 1.125 | 0.215 |
| 1 | 1 | 5 | 0.618 | 1.008 | 0.155 |
| 1 | 1 | 6 | 0.345 | 0.59 | 0.109 |
| 1 | 1 | 7 | 0.353 | 0.768 | 0.13 |
| 1 | 1 | 8 | 0.403 | 1.363 | 0.146 |
| 1 | 1 | 9 | 0.605 | 1 | 0.191 |
| 1 | 1 | 10 | 0.243 | 0.873 | 0.115 |
| 1 | 1 | 11 | 0.987 | 1.841 | 0.151 |
| 1 | 1 | 12 | 0.125 | 0.53 | 0.084 |
| 1 | 1 | 13 | 0.448 | 1.092 | 0.17 |
| 1 | 1 | 14 | 1.029 | 1.85 | 0.162 |
| 1 | 1 | 15 | 0.428 | 1.23 | 0.168 |
| 1 | 1 | 16 | 0.22 | 1.152 | 0.175 |

| | | | | | |
|---|---|---|---|---|---|
| 1 | 1 | 17 | 0.602 | 1.114 | 0.052 |
| 1 | 1 | 18 | 0.278 | 1.095 | 0.088 |
| 1 | 1 | 19 | 0.563 | 0.629 | 0.091 |
| 0 | 1 | 1 | 0.29 | 0.807 | 0.061 |
| 0 | 1 | 2 | 0.527 | 0.648 | 0.053 |
| 0 | 1 | 3 | 0.17 | 0.827 | 0.077 |
| 0 | 1 | 4 | 0.27 | 0.55 | 0.084 |
| 0 | 1 | 5 | 0.356 | 0.668 | 0.225 |
| 0 | 1 | 6 | 0.328 | 0.525 | 0.122 |
| 0 | 1 | 7 | 0.376 | 0.788 | 0.068 |
| 0 | 1 | 8 | 0.501 | 1.091 | 0.136 |
| 0 | 1 | 9 | 0.303 | 0.441 | 0.092 |
| 0 | 1 | 10 | 0.403 | 0.692 | 0.135 |
| 0 | 1 | 11 | 0.391 | 0.417 | 0.073 |
| 0 | 1 | 12 | 0.472 | 0.403 | 0.089 |
| 0 | 1 | 13 | 0.173 | 0.24 | 0.078 |
| 0 | 1 | 14 | 0.24 | 0.426 | 0.045 |
| 0 | 1 | 15 | 0.759 | 1.359 | 0.165 |
| 0 | 1 | 16 | 0.434 | 0.758 | 0.171 |
| 0 | 1 | 17 | 0.24 | 0.638 | 0.164 |
| 0 | 1 | 18 | 0.199 | 0.34 | 0.071 |
| 0 | 1 | 19 | 0.441 | 0.891 | 0.153 |
| 0 | 1 | 20 | 0.345 | 0.51 | 0.104 |
| 0 | 1 | 21 | 0.21 | 0.402 | 0.137 |
| 0 | 1 | 22 | 0.309 | 0.733 | 0.065 |
| 0 | 1 | 23 | 0.46 | 0.207 | 0.026 |
| 0 | 1 | 24 | 0.272 | 0.326 | 0.111 |
| 0 | 1 | 25 | 0.377 | 0.914 | 0.165 |
| 0 | 1 | 26 | 0.309 | 0.461 | 0.134 |
| 0 | 1 | 27 | 0.302 | 0.575 | 0.117 |
| 0 | 1 | 28 | 0.183 | 0.431 | 0.08 |
| 0 | 1 | 29 | 0.051 | 0.558 | 0.031 |
| 0 | 1 | 30 | 0.0597 | 0.795 | 0.186 |
| 0 | 1 | 31 | 0.274 | 0.367 | 0.063 |
| 0 | 1 | 32 | 0.54 | 0.613 | 0.042 |
| 0 | 1 | 33 | 0.206 | 0.354 | 0.066 |
| 0 | 1 | 34 | 0.11 | 0.858 | 0.017 |
| 0 | 1 | 35 | 0.241 | 0.864 | 0.081 |
| 0 | 1 | 36 | 0.322 | 0.417 | 0.103 |
| 0 | 1 | 37 | 0.365 | 0.71 | 0.08 |
| 0 | 1 | 38 | 0.257 | 0.362 | 0.076 |
| 0 | 1 | 39 | 0.45 | 0.768 | 0.01 |

| | | | | | |
|---|---|---|---|---|---|
| 0 | 1 | 40 | 0.3 | 0.483 | 0.067 |
| 0 | 1 | 41 | 0.247 | 0.526 | 0.05 |
| 0 | 1 | 42 | 0.346 | 0.842 | 0.055 |
| 0 | 1 | 43 | 0.26 | 0.767 | 0.063 |
| 0 | 1 | 44 | 0.513 | 0.529 | 0.098 |
| 0 | 1 | 45 | 0.314 | 0.348 | 0.7 |
| 0 | 2 | 1 | 0.29 | 0.406 | 0.023 |
| 0 | 2 | 2 | 0.247 | 0.928 | 0.071 |
| 0 | 2 | 3 | 0.216 | 0.576 | 0.077 |
| 0 | 2 | 4 | 0.287 | 0.54 | 0.069 |
| 0 | 2 | 5 | 0.212 | 0.362 | 0.035 |
| 0 | 2 | 6 | 0.276 | 0.336 | 0.065 |
| 0 | 2 | 7 | 0.145 | 0.168 | 0.072 |
| 0 | 2 | 8 | 0.169 | 0.302 | 0.05 |
| 0 | 2 | 9 | 0.162 | 0.321 | 0.04 |
| 0 | 2 | 10 | 0.201 | 0.841 | 0.057 |
| 0 | 2 | 11 | 0.755 | 1.089 | 0.254 |
| 0 | 2 | 12 | 0.651 | 0.862 | 0.19 |
| 0 | 2 | 13 | 0.131 | 0.867 | 0.041 |
| 0 | 2 | 14 | 0.177 | 0.25 | 0.059 |
| 0 | 2 | 15 | 0.268 | 0.275 | 0.034 |
| 0 | 2 | 16 | 0.227 | 0.83 | 0.04 |
| 0 | 2 | 17 | 0.321 | 0.403 | 0.042 |
| 0 | 2 | 18 | 0.267 | 1.15 | 0.105 |
| 0 | 2 | 19 | 0.28 | 0.438 | 0.08 |
| 0 | 2 | 20 | 0.304 | 0.634 | 0.123 |
| 0 | 2 | 21 | 0.515 | 0.898 | 0.2 |
| 0 | 2 | 22 | 0.345 | 0.371 | 0.109 |
| 0 | 2 | 23 | 0.325 | 0.614 | 0.056 |
| 0 | 2 | 24 | 0.616 | 1.064 | 0.06 |
| 0 | 2 | 25 | 0.137 | 0.521 | 0.051 |
| 0 | 2 | 26 | 0.241 | 0.534 | 0.06 |
| 0 | 2 | 27 | 0.165 | 0.668 | 0.059 |
| 0 | 2 | 28 | 0.203 | 0.519 | 0.046 |
| 0 | 2 | 29 | 0.329 | 0.329 | 0.031 |
| 0 | 2 | 30 | 0.188 | 0.741 | 0.052 |
| 0 | 2 | 31 | 0.251 | 0.658 | 0.102 |
| 0 | 2 | 32 | 0.272 | 0.378 | 0.09 |
| 0 | 2 | 33 | 0.182 | 0.233 | 0.032 |
| 0 | 2 | 34 | 0.53 | 0.736 | 0.117 |
| 0 | 2 | 35 | 0.297 | 1.214 | 0.101 |
| 0 | 2 | 36 | 0.247 | 0.331 | 0.07 |

| | | | | | |
|---|---|---|---|---|---|
| 0 | 2 | 37 | 0.342 | 0.495 | 0.095 |
| 0 | 2 | 38 | 0.158 | 0.59 | 0.04 |
| 0 | 2 | 39 | 0.403 | 0.915 | 0.1 |
| 0 | 2 | 40 | 0.29 | 0.525 | 0.073 |
| 0 | 2 | 41 | 0.119 | 0.179 | 0.023 |
| 0 | 2 | 42 | 0.715 | 0.874 | 0.035 |
| 0 | 2 | 43 | 0.384 | 0.85 | 0.119 |
| 0 | 2 | 44 | 0.2 | 1.264 | 0.126 |
| 0 | 2 | 45 | 0.351 | 0.594 | 0.03 |
| 0 | 2 | 46 | 0.34 | 0.442 | 0.1 |
| 0 | 2 | 47 | 0.104 | 0.211 | 0.032 |
| 0 | 2 | 48 | 0.106 | 0.312 | 0.04 |
| 0 | 2 | 49 | 0.078 | 0.324 | 0.04 |
| 0 | 2 | 50 | 0.119 | 0.357 | 0.016 |
| 0 | 2 | 51 | 0.561 | 0.692 | 0.046 |
| 0 | 2 | 52 | 0.187 | 0.452 | 0.023 |

**Results to Date: Crosstie Friction Experiments**

Ballast-crosstie friction experiments were conducted on a series of ballasts and crossties. A 24" section of crosstie is put on ballast material in a test stand capable of applying vertical and cyclic horizontal loads (see Figure 33). This work acquired data on the influence of ballast type, railroad tie, and moisture conditions influence the friction properties between the railroad track materials. The cases included permutations of:

- 3 types of ballast: 2 provided by BNSF and common gravel
- 4 crosstie types (wood, concrete, engineered polymer composite [EPC] – smooth and dimpled) provided by BNSF
- Varying normal load: 500 to 2000 lbs => equivalent to 2 to 8.5 kips on a 8'6" tie.
- Dry and wet.

Photos of the experiment are shown in Figure 34. Regarding the ballast support on the crosstie: No shoulder and minimal crib height. The typical lateral oscillations were 1.5 inches with a period of 60 to 80 seconds (back and forth), or ~0.4 inches/sec.

Cycles per test varied from a few dozen to 1200. Checks to ensure the test results were valid included observations of the variations in normal and horizontal forces and a comparison in push / pull forces (possibly indicating misalignment). The coefficient of friction (COF) was simply calculated as horizontal force / vertical force.

The reversals of direction in these tests often created movement of the ballast. Changes occur over ~0.10 inches (2 mm) and are sometimes accompanied by both normal load changes and horizontal load changes. Thus the coefficient of friction (COF) can change as illustrated in the cartoon in Figure 36 and the illustration in Figure 37 and an example case shown in Figure 38. It is noted that constant direction stopping and starting do not display these changes.

Tabulated results are shown in Table 7 through Table 12. As shown, the HDPE material without and with dimples has average COF values of 0.33 and 0.40. These values are relatively similar in wet conditions and seem to be within the standard deviations and experimental accuracy. The dry wood averages 0.23 while the wet wood has an average of 0.91 with peak COF values from 2 to 4.

This increase in the COF for wet wood appears consistent with the prior tests on the compressive properties of wet wood (lower stiffness and lower yield strength as compared with dry wood) and on the significant increase that is possible from individual ballast rocks penetrating deeper and creating significantly larger lateral resistance.

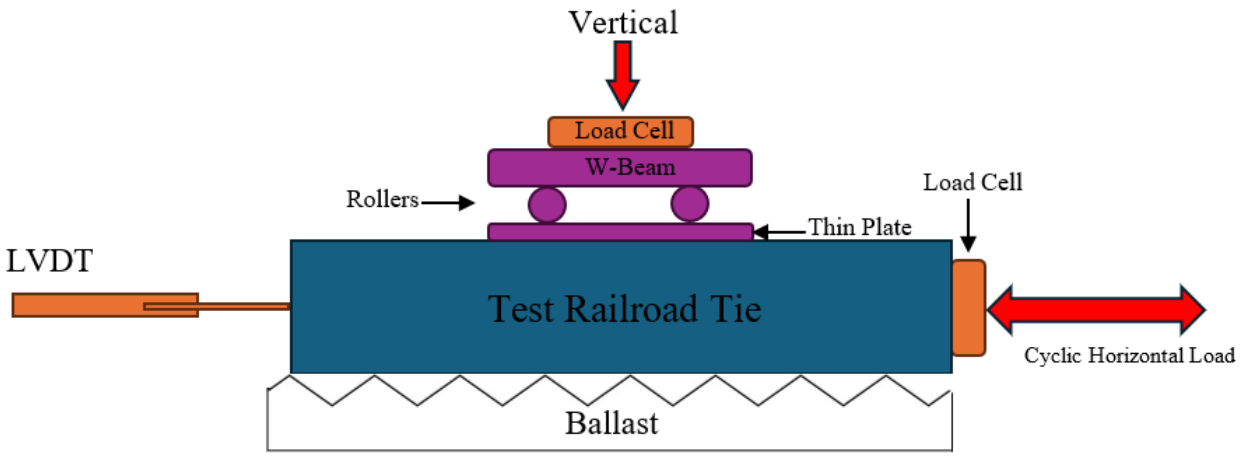


**Figure 33. Friction Test Configuration.**

**Figure 34. Photos of Friction Test Set-Up.**

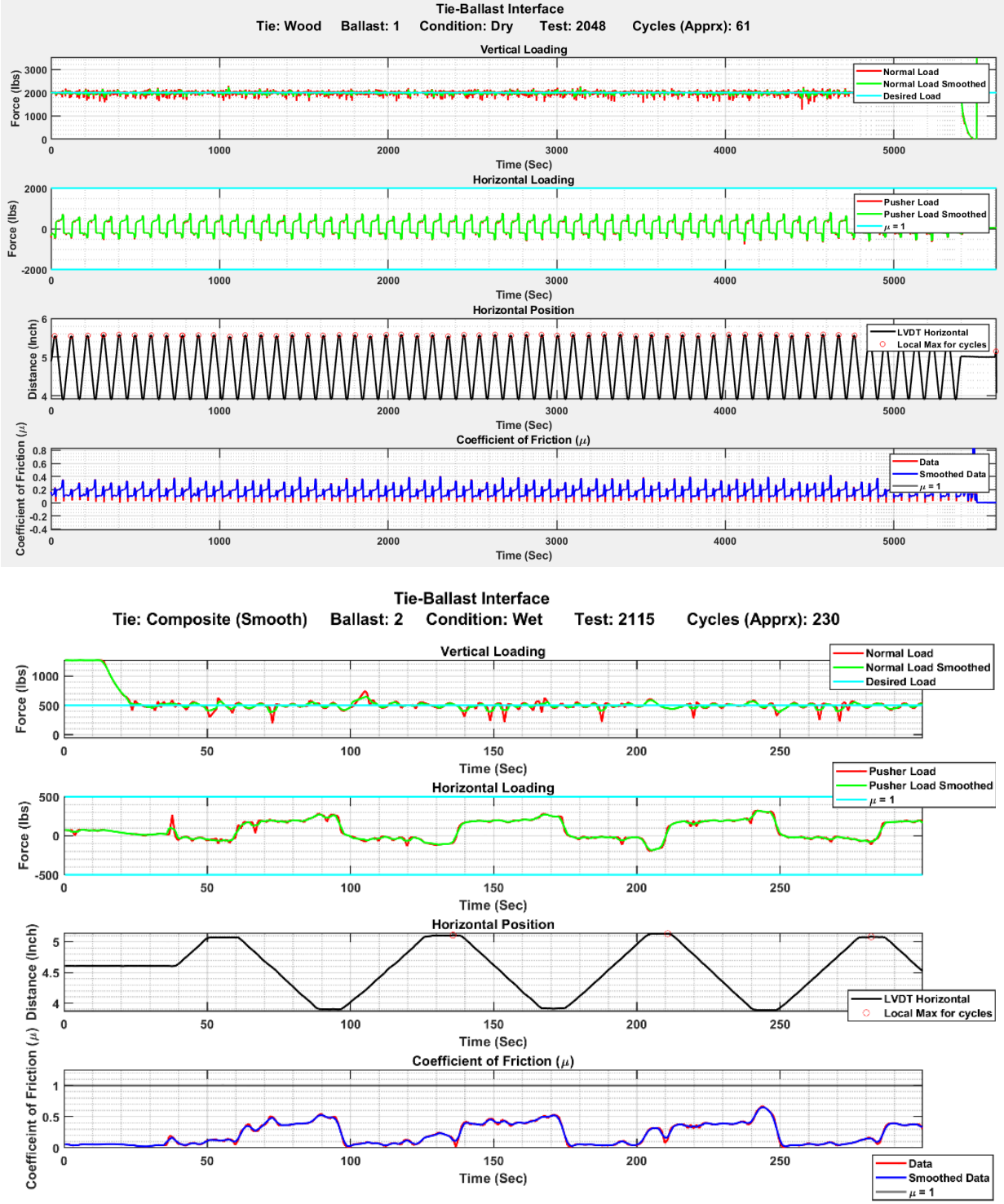


**Figure 35. Typical Outputs from Friction Experiment.**

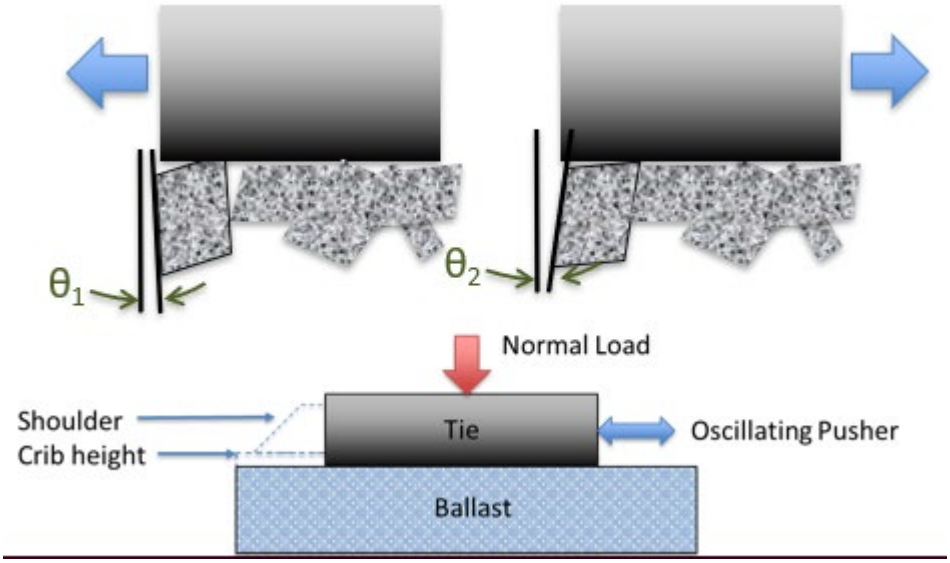


**Figure 36. Motion of Ballast During Tests.**

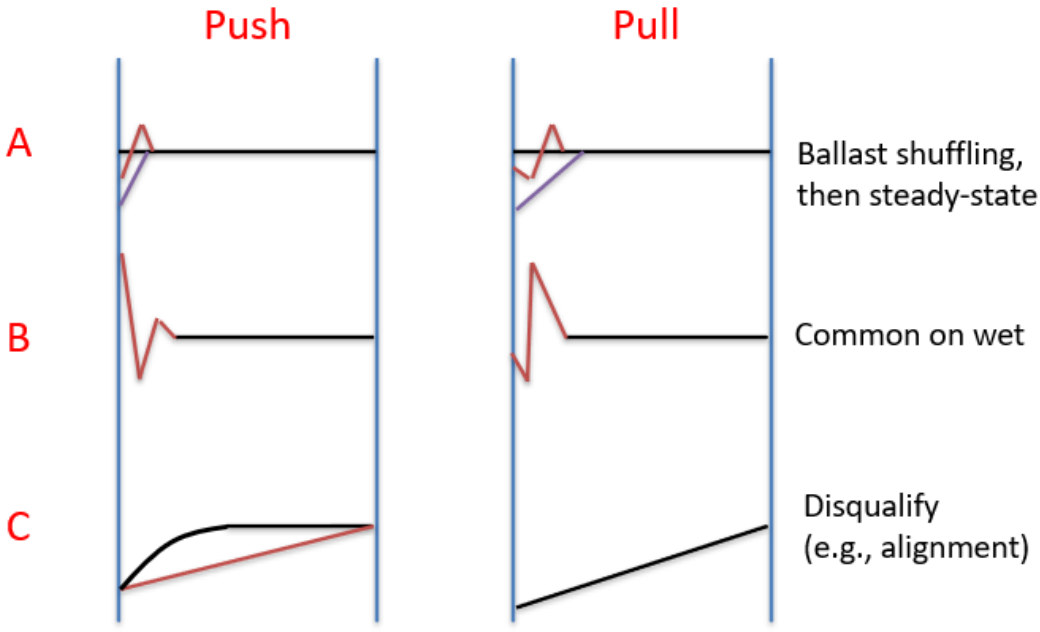


**Figure 37. Characteristic COF Patterns.**

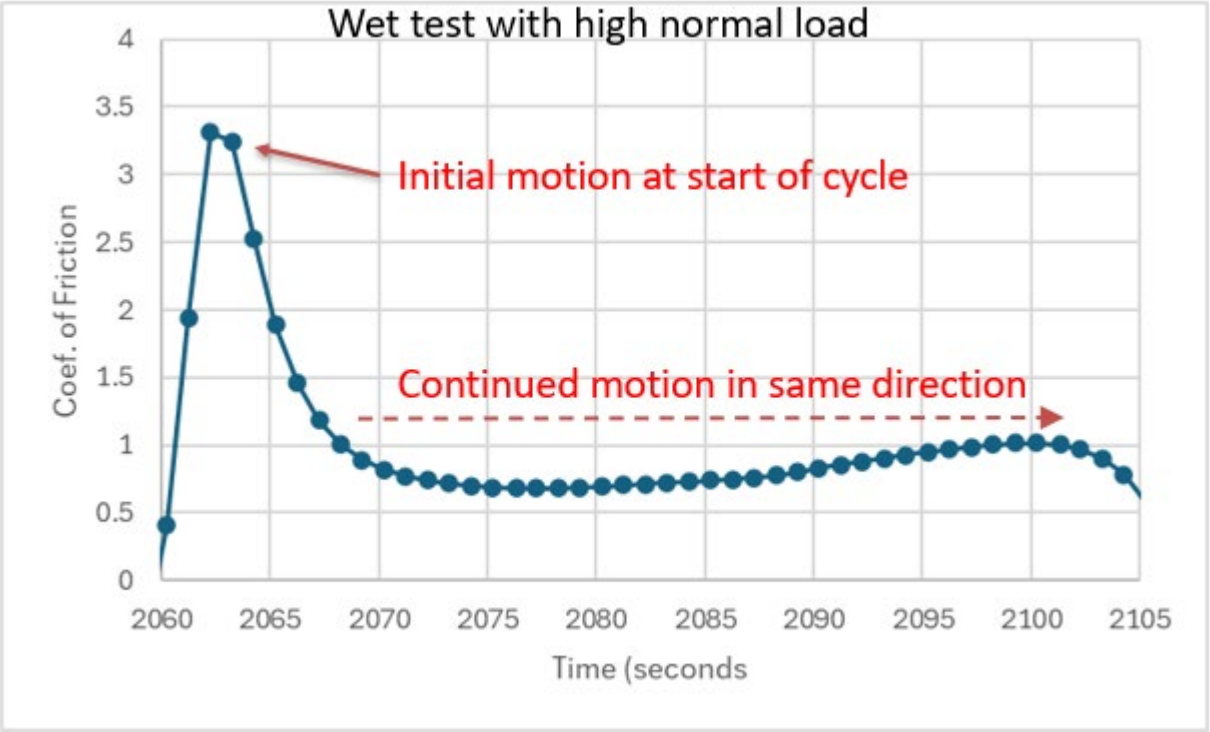


**Figure 38. Characteristic COF Pattern: Wet Wood Crosstie.**

**Table 7: COF Data: HDPE Composite Crosstie.**

| Test | Tie Material | # Cycles | COF: Mean | COF: Std. Dev. |
|---|---|---|---|---|
| 2030 | Composite Smooth | 96 | 0.30 | 0.07 |
| 2101 | Composite Smooth | 1052 | 0.35 | 0.05 |
| 2102 | Composite Smooth | 70 | 0.32 | 0.03 |
| 2104 | Composite Smooth | 505 | 0.34 | 0.04 |
| 2105 | Composite Smooth | 414 | 0.30 | 0.05 |
| 2111 | Composite Smooth | 197 | 0.32 | 0.08 |

**Average: 0.33**

**Table 8: COF Data: HDPE Composite Crosstie with Dimples.**

| Test | Tie Material | # Cycles | COF: Mean | COF: Std. Dev. |
|---|---|---|---|---|
| 2032 | Composite Dimples | 218 | 0.45 | 0.12 |
| 2035 | Composite Dimples | 32 | 0.59 | 0.14 |
| 2038 | Composite Dimples | 263 | 0.37 | 0.04 |
| 2094 | Composite Dimples | 81 | 0.34 | 0.06 |
| 2095 | Composite Dimples | 139 | 0.34 | 0.06 |
| 2096 | Composite Dimples | 124 | 0.33 | 0.06 |
| 2097 | Composite Dimples | 83 | 0.46 | 0.09 |
| 2098 | Composite Dimples | 159 | 0.45 | 0.10 |
| 2099 | Composite Dimples | 114 | 0.38 | 0.08 |
| 2100 | Composite Dimples | 142 | 0.43 | 0.08 |

Average: 0.40

**Table 9: COF Data: Dry Wood Crosstie.**

| Test | Tie Material | # Cycles | COF: Mean | COF: Std. Dev. |
|---|---|---|---|---|
| 2042 | Wood | 239 | 0.25 | 0.02 |
| 2044 | Wood | 61 | 0.15 | 0.01 |
| 2045 | Wood | 202 | 0.16 | 0.03 |
| 2079 | Wood | 189 | 0.24 | 0.05 |
| 2080 | Wood | 1167 | 0.21 | 0.03 |
| 2081 | Wood | 621 | 0.19 | 0.03 |
| 2082 | Wood | 47 | 0.21 | 0.03 |
| 2084 | Wood | 1047 | 0.24 | 0.04 |
| 2085 | Wood | 40 | 0.60 | 0.08 |
| 2086 | Wood | 231 | 0.38 | 0.05 |

Average: 0.23

**Table 10: COF Data: Wet HDPE Composite Crosstie.**

| Test | Tie Material | # Cycles | COF: Mean | COF: Std. Dev. |
|---|---|---|---|---|
| 2063 | Composite Smooth | 98 | 0.38 | 0.08 |
| 2064 | Composite Smooth | 305 | 0.31 | 0.04 |
| 2066 | Composite Smooth | 883 | 0.29 | 0.04 |
| 2067 | Composite Smooth | 924 | 0.26 | 0.04 |
| 2112 | Composite Smooth | 285 | 0.25 | 0.05 |
| 2113 | Composite Smooth | 334 | 0.23 | 0.04 |
| 2114 | Composite Smooth | 233 | 0.22 | 0.04 |
| 2115 | Composite Smooth | 230 | 0.21 | 0.04 |
| 2116 | Composite Smooth | 324 | 0.22 | 0.04 |
| 2117 | Composite Smooth | 137 | 0.41 | 0.06 |
| 2119 | Composite Smooth | 310 | 0.23 | 0.06 |

Average: 0.26

**Table 11: COF Data: Wet HDPE Composite Crosstie with Dimples.**

| Test | Tie Material | # Cycles | COF: Mean | COF: Std. Dev. |
|---|---|---|---|---|
| 2072 | Composite Dimples | 420 | 0.41 | 0.07 |
| 2073 | Composite Dimples | 480 | 0.36 | 0.06 |
| 2074 | Composite Dimples | 140 | 0.57 | 0.08 |
| 2075 | Composite Dimples | 162 | 0.51 | 0.06 |
| 2077 | Composite Dimples | 567 | 0.44 | 0.06 |
| 2078 | Composite Dimples | 187 | 0.40 | 0.06 |
| 2120 | Composite Dimples | 82 | 0.46 | 0.10 |
| 2121 | Composite Dimples | 5 | 0.41 | 0.07 |
| 2122 | Composite Dimples | 185 | 0.36 | 0.05 |
| 2123 | Composite Dimples | 200 | 0.32 | 0.05 |
| 2124 | Composite Dimples | 170 | 0.31 | 0.06 |

Average: 0.41

**Table 12: COF Data: Wet Wood Crosstie.**

| Test | Tie Material | # Cycles | COF: Mean | COF: Std. Dev. | Notes |
|---|---|---|---|---|---|
| 2052 | Wood | 82 | 0.87 | 0.31 | Wet peak COF of 2 to 4. |
| 2059 | Wood | 48 | 1.24 | 0.60 | |
| 2060 | Wood | 98 | 0.84 | 0.21 | |
| 2061 | Wood | 119 | 0.83 | 0.36 | |
| 2062 | Wood | 209 | 0.93 | 0.27 | |
| 2125 | Wood | 11 | 0.88 | 0.19 | |
| 2128 | Wood | 177 | 0.93 | 0.30 | |
| 2129 | Wood | 198 | 0.91 | 0.29 | |
| 2130 | Wood | 35 | 0.88 | 0.19 | |
| 2132 | Wood | 38 | 0.77 | 0.26 | |

Average: 0.91


**Results to Date: Implications and Discussion**

Several tests and finite element models were examined to better understand the properties within a rail support system. The investigation also focused on the local behavior of a single indenter (rock) on a crosstie. Since the penetration depth greatly influences the lateral resistance, the compressive properties of the crossties had to be determined. For wood crossties, this meant testing compressive properties perpendicular to the grain direction, a value that is uncommon and does not have a widespread basis or expected value.

The ballast characteristics are believed to play a significant role in the lateral resistance of a crosstie. This work examined common gravel, with a significantly smaller average volume than standard ballast. The common gravel is believed to support the crosstie well, but provide relatively less lateral resistance because of the larger volume ballast rocks that dig into the crossties, especially if they are pointed or faceted.

The friction experiments displayed differences between HDPE crossties and HDPE crossties with dimples. As expected from the single-indention finite element models, geometric bumps create a situation in which the indenter (rock) is basically buried and the lateral resistance increases substantially. While not examined yet, this may also be important to concrete ties (see Figure 39) that are not expected to have significant sliding resistance on ballast (because the rocks

are unlikely to penetrate the concrete) but they create significant resistance from the cavity on the underside of the tie, especially when tamped.

The results also have implications for aging track. Several studies have examined ballast wear. The focus of the experimental work on the coefficients of friction did not record wear or document fines produces from rock-on-rock abrasion. Graphs such as the one shown in Figure 40 do show a difference in early and late cycles and could be used with a wear model to capture the rate of wear and the effect on the friction. In the lab, evidence of crosstie wear has been observed on HDPE and wet wood crossties (see Figure 41).

Future work will continue refining the distributions of properties mentioned in this report. Simple preliminary modeling also indicates a reasonable prediction for single tie push tests (STPT) results based on (a) the indents per inch (which are a function of ballast volume), (b) the distribution of indent diameters and depths (which are a function of ballast size and facetedness, and load per indent), and (c) the lateral resistance (stemming from, for example, the finite element modeling of a single indenter moving laterally with an estimated friction.

Additional future work is being planned to understand the effect of side friction on the sides of a crosstie, with and without tamping. The presence of a ballast forming around the crosstie, a crib, or a shoulder needs to also be examined.

**Figure 39. Concrete Crosstie at Texas A&M for Testing.**

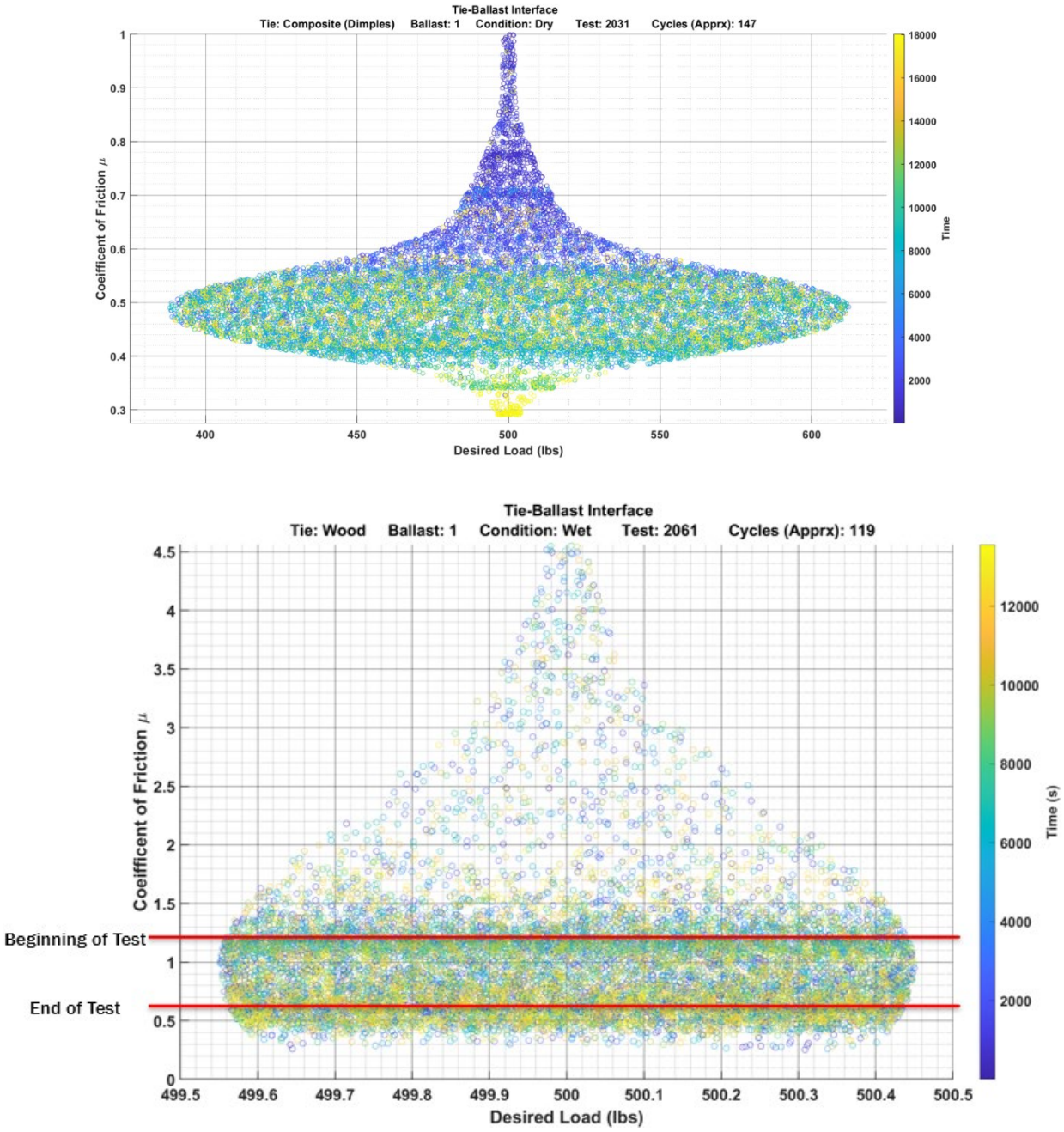


**Figure 40. Swarm Plot of Friction over Time Showing Friction Change.**

**Figure 41. Wear on HDPE Crosstie.**

## References


1. Musu, V. "Development of a Model for the Prediction of the Effects of Multiple Distinct Modes of Nonlinearity on Rail Buckling," Texas A&M Thesis, 2023.
2. Saberi, S., G. Whetstone, and D. H. Allen. Multiscale Computational Modeling of Subsurface Cracking in Railhead: Insights Into Fatigue Life. No. 87776, 2024, pp. V001T05A002.
3. Whetstone, G., T. Liu, P. Fudlailah, C. V. Droddy, and D. H. Allen. Experimental Evaluation of Crack Evolution in Rails Using a Phased Array. Journal of Nondestructive Evaluation, Vol. 42, No. 4, 2023. https://doi.org/10.1007/s10921-023-00997-z.
4. BNSF Railway Company, "Guidelines for Industry Track Projects," July, 2023.
5. Chow, P., et al., "Proposed Strength Property Tests for Wood Crossties," Crossties, 1995.
6. "The Tie Guide: Handbook for Commercial Timbers Used by the Railroad Industry," edited by J. C. Gauntt.
7. Ticoalu, A, Aravinthan, T., and Karunasena, W, "An investigation on the stiffness of timber sleepers for the design of fibre composite sleepers," 2008.
8. US Dept. of Transportation, Federal Railroad Administration, "Cracking and Impact Performance Characteristics of Plastic Composite Ties," March 2012.
9. Lotfy, I, and Issa, M, "Evaluation of the longitudinal restraint, uplift resistance, and long-term performance of high-density polyethylene crosstie rail support system using static and cyclic loading," Journal of Rail and Rapid Transit, 2017.
10. McHenry, M, Gao, Y, and Baillargeon, J, "Implementing improved composite tie design and testing guidelines into the AREMA manual for railway engineering," AREMA 2018.